We scratched wounds in the cell monolayer using a sterile 200-μl pipet tip, rinsed the cells with phosphate-buffered saline and added DMEM containing 10% FCS with or without mitomycin C (10 μg/ml, Nacalai Tesque, Kyoto, Japan). Cells were allowed to migrate into the wound for 0, 12, or 24 h before fixation. Cells were stained with Giemsa stain (Nacalai Tesque) or were triple-labeled with anti-p190-B RhoGAP, rhodamine-phalloidin and DAPI as described above. Wound widths were measured in three randomly chosen regions. Experiments were repeated at least three times.

2.10. Statistical analysis

Analysis of variance (ANOVA) was performed using SPSS 15.0 software (SPSS Inc., Chicago, IL, USA). *P* values of <0.05 were considered significant.

3. Results

3.1. Detection of 14q12 amplicon in HCC and ESCC cell lines by array analyses

We screened for DNA copy number aberrations in 10 HCC cell lines and 10 ESCC cell lines using GeneChip Mapping 250 K array analysis. Of the 20 cell lines, one HCC cell line, Huh-7, and two ESCC cell lines, T.T and TE-4, commonly exhibited copy number gains at chromosomal region 14q12 (Fig. 1A). In particular, Huh-7 cells showed a high-level gain indicative of amplification in a narrow region on 14q12 between the positions recognized by the Affymetrix SNP_A-1933754 and SNP_A-2088149 probes. To confirm amplification in Huh-7 cells, we performed FISH analyses using BACs RP11-113E19, RP11-431H16 and RP11-54H22 as probes (Fig. 1B–D). BAC RP11-431H16 generated strong signals as a small homogeneously staining region (HSR), indicating amplification (Figs. 1C, D). In contrast, BACs RP11-113E19 or RP11-54H22 did not show a HSR pattern, indicating their positions outside the amplicon (Fig. 1C and D). Furthermore, we determined gene dosages in Huh-7 cells at the STS markers RH53739, SHGC32910, SHGC24139, G36143, D14S941, RH45106, and RH45526 loci by real time quantitative PCR. (Fig.1B and E). The highest copy number was observed at the D14S941 and RH45106 loci. Taken together, we defined the smallest region of amplification between markers G36143 and RH45526. The extent of the amplicon was estimated to be 1.2 Mb. This region includes four known or predicted protein-coding genes, *HEATR5A*, *c14orf126*, *NUBPL*, and *ARHGAP5*.

3.2. Identification of candidate target genes in the 14q12 amplicon

The 14q12 region may harbor one or more genes (henceforth called 'target genes') that, when activated by amplification, play a role in carcinogenesis. A common criterion for designating a gene as a putative target is that amplification leads to its overexpression [8]. Using real-time quantitative PCR, we determined mRNA levels of all four genes within the amplicon in the 10 HCC cell lines and 10 ESCC cell lines. Among the four genes, *HEATR5A* and *ARHGAP5* were commonly overexpressed in Huh-7, T.T and TE-4 cells, the cell lines that were found to have copy number gains at 14q12 (Fig. 2A). These findings identified *ARHGAP5*, which encodes p190-B RhoGAP, as one of candidate target genes for the 14q12 amplicon.

We determined copy numbers of *ARHGAP5* in the 10 HCC and 10 ESCC cell lines by real-time quantitative PCR (Fig. 2B). Copy number changes were counted as gains if the results of the analysis for a given tumor cell type exceeded the twofold levels of the gene in normal cells. A copy number gain of *ARHGAP5* was observed in six (30%) of the 20 cell lines: Huh-7, T.T, KYSE140, TE-4, TE-6 and TE-10.

We examined the expression of p190-B RhoGAP protein in 4 HCC and 4 ESCC cell lines by immunoblot analysis. As shown in Fig. 2C, expression levels of p190-B RhoGAP were higher in cell lines exhibiting copy number gains of *ARHGAP5* (Huh-7, T.T, KYSE140, TE-4 and TE-10) than other cell lines that did not show gains (SNU354, Huh-1 and PLC/PRF/5).

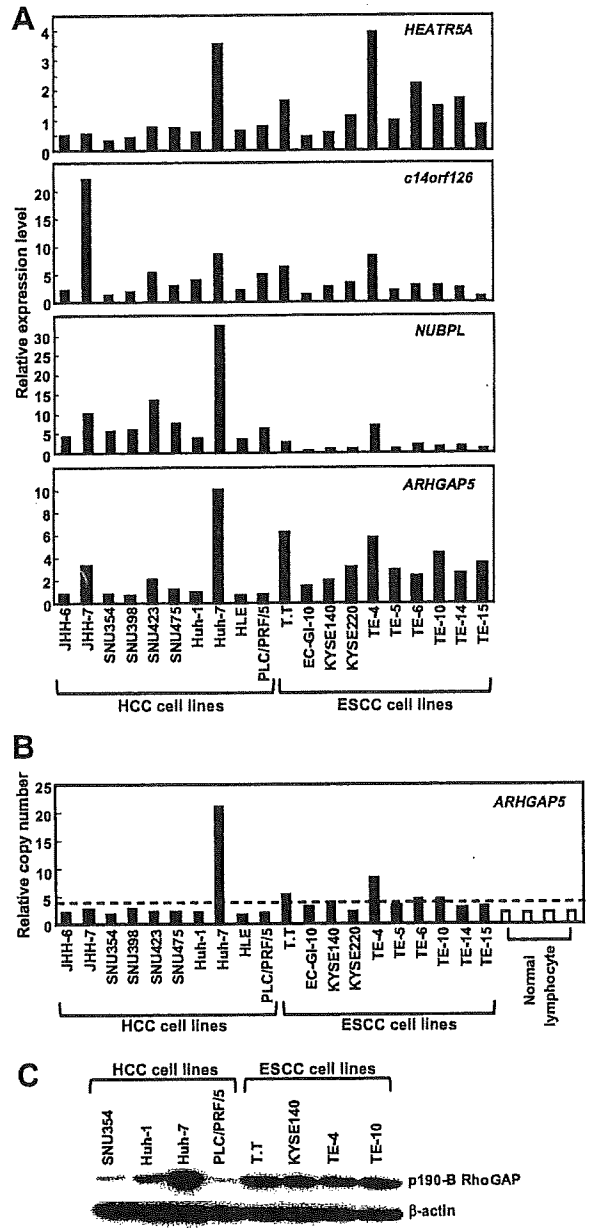

Fig. 2. Amplification and overexpression of *ARHGAP5* in Huh-7, T.T and TE-4 cell lines. (A) Relative expression levels of four genes (*HEATR5A*, *c14orf126*, *NUBPL* and *ARHGAP5*) within the 14q12 amplicon in 10 HCC and 10 ESCC cell lines as evaluated by real-time quantitative PCR. Results are presented as expression levels of each gene relative to a reference gene (*GAPDH*) to correct for variations in the amount of RNA. (B) Copy numbers at the *ARHGAP5* locus (the STS marker RH45106) in 10 HCC cell lines, 10 ESCC cell lines and four normal peripheral blood lymphocytes as measured by real-time quantitative PCR with reference to LINE-1 controls. Values are normalized such that the average copy number in genomic DNA derived from four normal lymphocytes has a value of 2. A value of 4, which is a twofold increase in copy number of normal lymphocytes, was used to determine the cut-off value for copy number gain, shown as a dotted line. (C) Levels of p190-B RhoGAP and β-actin, an internal control, determined by immunoblotting in 4 HCC and 4 ESCC cell lines.

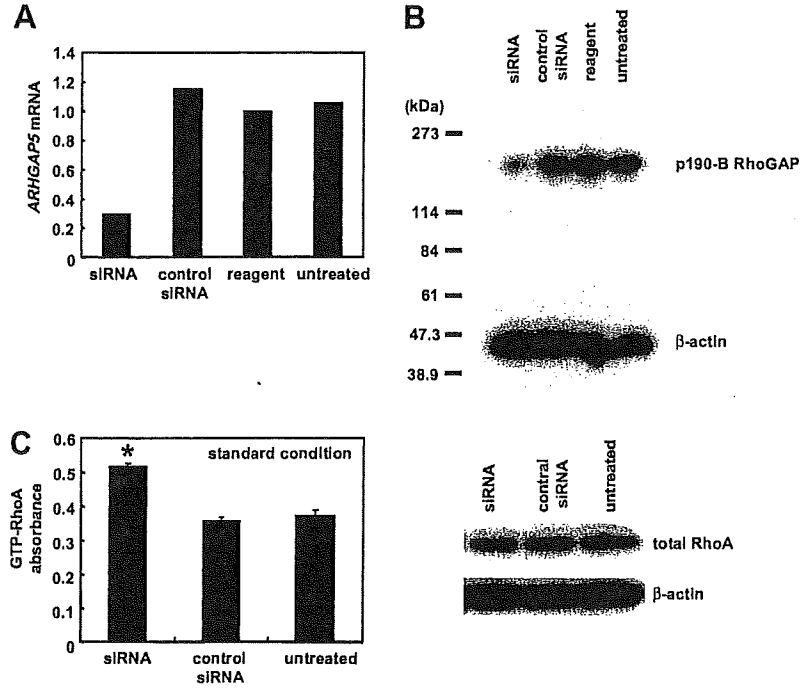

Fig. 3. Knockdown of *ARHGAP5* increases RhoA activity. (A) Relative expression levels of *ARHGAP5* mRNA as determined by real-time quantitative PCR. Huh-7 cells were treated with siRNA targeting *ARHGAP5*, negative control siRNA or transfection agent alone. Untreated cells were maintained under identical experimental conditions. Results are presented as a ratio between the expression level of *ARHGAP5* and that of a reference gene (*GAPDH*) to correct for variation in the amount of RNA. Relative expression levels were normalized such that the ratio in untreated cells was 1. (B) Levels of p190-B RhoGAP and β-actin, an internal control, determined by immunoblotting. (C) (*left*) Levels of RhoA activity under standard culture conditions (DMEM containing 10% FCS). RhoA activity was measured using a G-LISA kit (see Methods section). Values are represented as the mean ± S.D. Differences were analyzed by ANOVA ($^*P < 0.05$). (*right*) Total RhoA and β-actin were determined by immunoblotting.

3.3. Regulation of RhoA activity by p190-B RhoGAP in Huh-7 cells

To investigate the biological function of p190-B RhoGAP in HCC cells, knockdown of *ARHGAP5* expression in Huh-7 cells was carried out using RNAi. Following treatment of Huh-7 cells with siRNA targeting *ARHGAP5*, we observed a decrease in both *ARHGAP5* mRNA and p190-B RhoGAP protein levels relative to what was observed for cells receiving control siRNA, transfection agent alone or left untreated (Fig. 3A and B). Because p190-B RhoGAP negatively regulates RhoA activity, we examined the effect of the siRNA-mediated knockdown of *ARHGAP5* on RhoA activity. Huh-7 cells were treated with *ARHGAP5* siRNA or control siRNA or were left untreated. Cells were then cultured in DMEM containing 10% FCS for 48 h under standard conditions. RhoA activity levels were higher in cells treated with *ARHGAP5* siRNA than in cells treated with control siRNA or in untreated cells, whereas total RhoA levels were similar among the three groups (Fig. 3C). These findings suggest that overexpression of *ARHGAP5* contributes to downregulation of RhoA activity in Huh-7 cells.

3.4. Regulation of cell spreading by p190-B RhoGAP in Huh-7 cells

It is known that integrin-mediated adhesion regulates the activity of p190-B RhoGAP and RhoA [3,9]. We therefore examined the function of p190-B RhoGAP when Huh-7 cells were plated on fibronectin, a specific ligand for α5β1 integrin. Huh-7 cells treated with *ARHGAP5* siRNA or control siRNA or left untreated were suspended and plated on fibronectin. Prior to and during plating, cells were maintained in DMEM containing 1% FCS. Adhesion to fibronectin regulated RhoA activity in a triphasic or biphasic manner (Fig. 4A). Prior to plating (0 min), RhoA activity was significantly higher in *ARHGAP5* siRNA-treated cells than in control siRNA-treated cells or untreated cells. In *ARHGAP5* siRNA-treated cells, RhoA activity rapidly and transiently decreased (20 min). This initial decline was followed by an increase that peaked at 60 min. In the final phase, RhoA activity gradually decreased. In control siRNA-treated cells or untreated cells, an initial period of low RhoA activity was followed by a slight increase that peaked between 40–60 min and then returned to basal level. RhoA activity was significantly higher in *ARHGAP5* siRNA-treated cells than control siRNA-treated cells or untreated cells between 40 and 180 min. During the experimental period, expression of p190-B RhoGAP was continuously knocked down by *ARHGAP5* siRNA and total RhoA levels were similar among the three groups (Fig. 4A).

Because RhoA affects cell motility by stimulating reorganization of actin, we examined whether p190-B RhoGAP regulates the spreading of Huh-7 cells on fibronectin. Using immunofluorescence, we observed morphological changes in Huh-7 cells during attachment and spreading on fibronectin (Fig. 4B). Phalloidin staining revealed that *ARHGAP5* siRNA-treated cells exhibited more robust actin stress fibers but less membrane ruffling and protrusion at the cell periphery than control siRNA-treated cells or untreated cells. The actin stress fiber formation and reduced membrane ruffling and protrusion observed in *ARHGAP5* siRNA-treated cells corresponded with higher RhoA activity (Fig. 4)

p190-B RhoGAP was expressed diffusely in the cytoplasm of control siRNA-treated cells and untreated cells, whereas it was hardly detected in *ARHGAP5* siRNA-treated cells. We found that p190-B RhoGAP had partially translocated to the membrane protrusions in control siRNA-treated cells and untreated cells by 40 min after plating (Fig. 4B). Taken together, these findings suggest that RhoA inactivation by p190-B RhoGAP results in inhibition of actin stress fiber formation, enhanced membrane ruffling and protrusion and promotion of cell spreading on fibronectin.

3.5. Regulation of cell migration by p190-B RhoGAP in Huh-7 cells

To investigate the role of p190-B RhoGAP in cell motility, we performed a monolayer wound healing assay. Wound closure was delayed in *ARHGAP5* siRNA-treated cells relative to control siRNA-treated cells or untreated cells, whether cultured in the presence of mitomycin C or in its absence (Figs. 5A–E). Mitomycin C blocks mitosis and thus allows analysis of cell migration in the absence of cell proliferation. These results show that cell migration, rather than cell proliferation, is the major factor

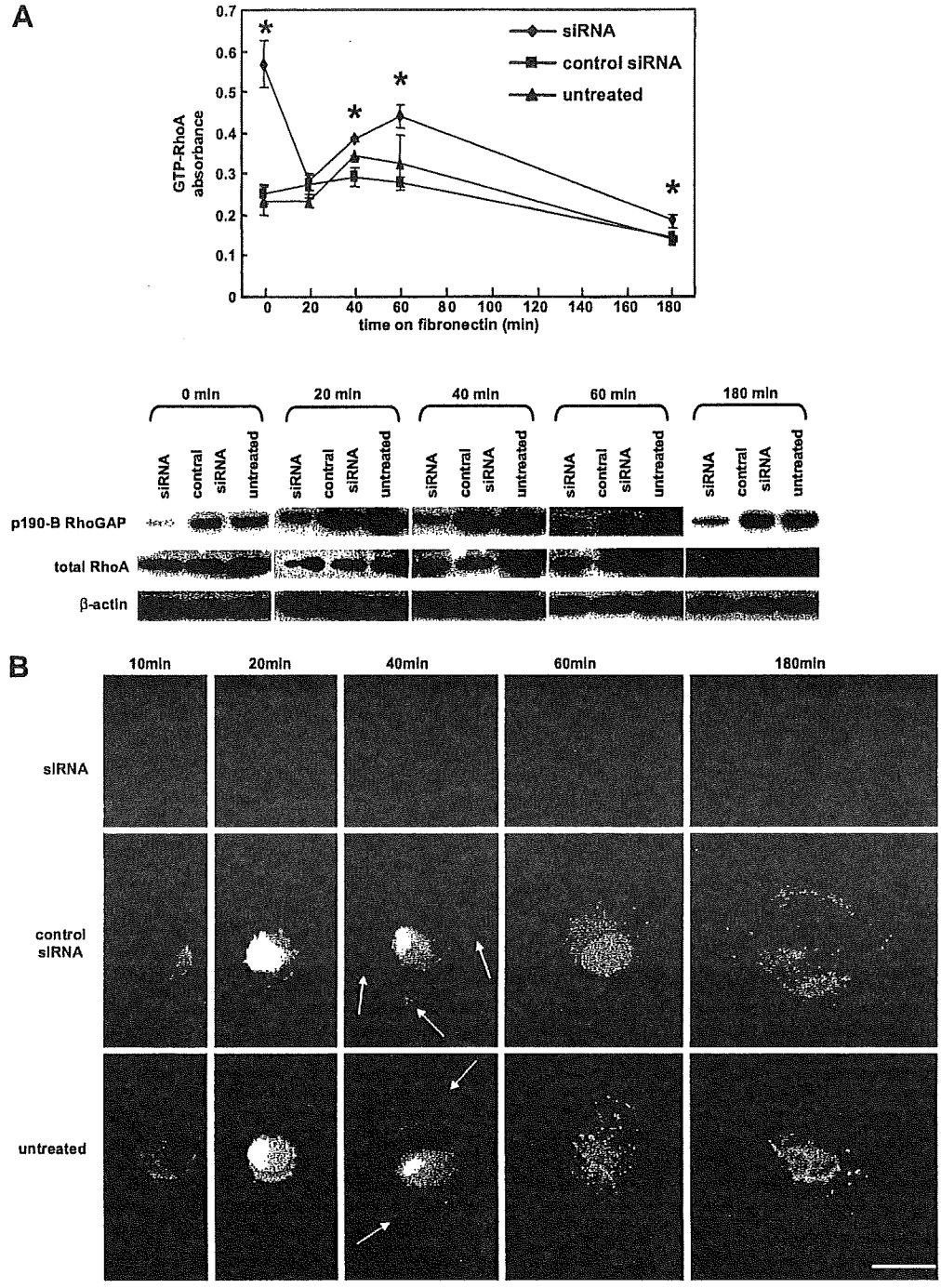

Fig. 4. Knockdown of *ARHGAP5* inhibits Huh-7 cell spreading on fibronectin. (A) Time course of changes in RhoA activity (*upper*) and levels of p190-B RhoGAP and total RhoA (*lower*). Huh-7 cells treated with siRNA targeting *ARHGAP5* or control siRNA or left untreated were plated on fibronectin as described in Materials and Methods and harvested at the indicated time points. Values of RhoA activity are represented as the mean ± SD. Differences were analyzed by ANOVA ($^{*}P < 0.05$). Levels of p190-B RhoGAP, total RhoA and β-actin were determined by immunoblotting. (B) Time course of cell spreading on fibronectin. Huh-7 cells treated with siRNA targeting *ARHGAP5* or control siRNA or left untreated were plated on fibronectin, fixed at the indicated time points and then triple-labeled with anti-p190-B RhoGAP, rhodamine-conjugated phalloidin and DAPI to reveal p190-B RhoGAP (green), actin filaments (red), and nuclei (blue), respectively. Arrows indicate p190-B RhoGAP on membrane protrusions. Scale bar = 10 μm.

in the retarded wound repair process in *ARHGAP5* siRNA-treated cells. Wound edge cells in *ARHGAP5* siRNA-treated cells had more abundant actin stress fibers but less membrane ruffling and protrusion at the leading edge than control siRNA-treated or untreated cells (Figs. 5F–H). p190-B RhoGAP translocated to the membrane protrusions of control siRNA-treated or untreated cells at the edge of the wound, but not in *ARHGAP5*-siR-

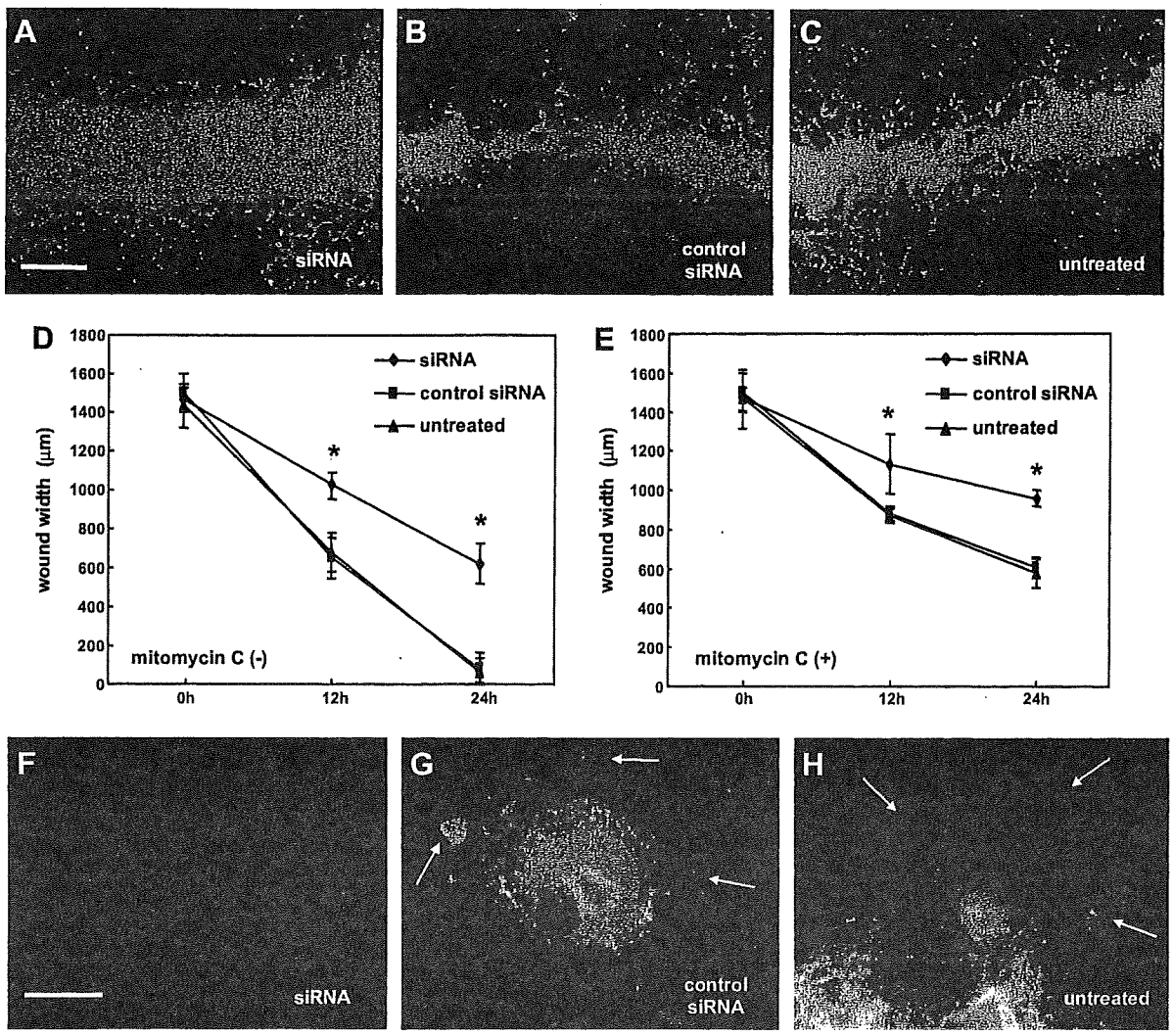

Fig. 5. Knockdown of *ARHGAP5* inhibits migration in Huh-7 cells. Monolayer wound healing assay in Huh-7 cells transfected with siRNA targeting *ARHGAP5* (A, F) or control siRNA (B and G), or left untreated (C and H). Cells were cultured in the absence (A–D, F–H) or presence (E) of mitomycin C. (A–C) Cells were allowed to migrate into a monolayer wound for 24 h and afterward stained with Giemsa stain. Original magnifications: 40×. Scale bar = 500 μm. (D and E) Cells were cultured in the absence (D) or presence (E) of mitomycin C. Wound widths were measured in three randomly chosen regions at the indicated time after wounding. Values are represented as the mean ± SD. Differences were analyzed by ANOVA ($^*P < 0.05$). (F–H) Wound edge cells were triple-labeled with anti-p190-B RhoGAP, rhodamine-conjugated phalloidin and DAPI to reveal p190-B RhoGAP (green), actin filaments (red) and nuclei (blue), respectively. Arrows indicate p190-B RhoGAP on membrane protrusions. Scale bar = 10 μm.

NA cells. Taken together, these observations suggest that the inhibition of RhoA activity by p190-B RhoGAP promotes cell movement and formation of membrane protrusions in migrating cells.

4. Discussion

We report here the amplification of *ARHGAP5* in HCC and ESCC cell lines. We undertook a molecular definition of the amplicon at 14q12 that is present in HCC and ESCC cell lines. The amplification at 14q12 has been reported in various types of cancers, including HCC [10], ESCC [7], nasopharyngeal carcinoma [11] and non-squamous cell lung carcinoma [12], although the frequency of 14q12 gain is low in primary HCC (4–6%) [10,13]. The range of the amplicon varies among these tumors, and their boundaries have not been determined in each case. Moreover, the target oncogene(s) in the amplified regions have not been fully identified. Here we defined the amplified regions in one HCC and two ESCC cell lines and narrowed the site of the amplification to a relatively short section. Among the four genes within the smallest region of the amplification, only *HEATR5A* and *ARHGAP5* were overexpressed in all the tested lines exhibiting copy number gains in the region; hence they are thought to be candidate targets in the amplicon. Of the two genes, we chose to focus further analysis on *ARHGAP5* because its protein product, p190-B RhoGAP, is purported to play an important role in dynamic cellular processes by regulating RhoA activity, while little is known about *HEATR5A*. During the preparation of this manuscript, amplification of *ARHGAP5* was reported in Huh-7 cells [14].

Although several studies have suggested an association of p190-B RhoGAP with tumors [15–17], its biological function in cancer cells is poorly understood. Therefore, using siRNA, we studied its function in Huh-7 cells, the HCC cell line that exhibited the most remarkable copy number gain and overexpression of *ARHGAP5*. We found that p190-B RhoGAP negatively regulates RhoA activity in Huh-7 cells cultured in medium containing 10% FCS and plated on fibronectin. Adhesion to fibronectin regulated RhoA activity in a triphasic or biphasic manner, as previously reported in fibroblasts [18,19]. Although some RhoA activity is required for migration, possibly to maintain sufficient adhesion to the substrate, high activity inhibits movement [19–22]. Our results showed that RhoA inactivation by p190-B RhoGAP results in inhibition of actin stress fiber formation, enhanced membrane ruffling and protrusion, and promotion of spreading and migration of Huh-7 cells. These findings are in agreement with results obtained from previous studies. A dominant negative (loss-of-function) p190-B RhoGAP mutation elevates RhoA activity in fibroblasts cultured on fibronectin and inhibits their migration, whereas overexpression of wild-type p190-B RhoGAP decreases RhoA activity, promotes the formation of membrane protrusions and enhances mobility [19]. Activation of β1 integrin signaling stimulates tyrosine phosphorylation of p190-B RhoGAP and promotes membrane protrusion at invadopodia in a melanoma cell line [17]. p190-B RhoGAP is also involved in invasion by breast cancer cells [15].

In conclusion, we have identified *ARHGAP5* as a probable target for the amplification at 14q12 detected in a subgroup of HCCs and ESCCs. Our results indicate that p190-B RhoGAP, the protein product of *ARHGAP5*, promotes cell spreading and migration in Huh-7 cells. Further studies are needed to determine the importance of *ARHGAP5* and p190-B RhoGAP in the development and progression of not only HCC and ESCC but also other types of tumors.

Conflicts of interest statement

My co-authors and I declare that we have no proprietary, financial, professional or other personal interest of any nature or kind in any product, service and/or company that could be construed as influencing the position presented in the manuscript entitled, "A novel amplification target, ARHGAP5, promotes cell spreading and migration by negatively regulating RhoA in Huh-7 hepatocellular carcinoma cells".

Acknowledgements

Supported by: Grants-in-Aid for Scientific Research (18390223) from the Japan Society for the Program of Science (to K.Yasui).

References

[1] A. Hall, Rho GTPases and the actin cytoskeleton, Science 279 (1998) 509–514.
[2] P.D. Burbelo, S. Miyamoto, A. Utani, S. Brill, K.M. Yamada, A. Hall, Y. Yamada, P190-B, a new member of the Rho GAP family, and Rho are induced to cluster after integrin cross-linking, J. Biol. Chem. 270 (1995) 30919–30926.
[3] W.T. Arthur, L.A. Petch, K. Burridge, Integrin engagement suppresses RhoA activity via a c-Src-dependent mechanism, Curr. Biol. 10 (2000) 719–722.
[4] G.C. Kennedy, H. Matsuzaki, S. Dong, W.N. Liu, J. Huang, G. Liu, X. Su, M. Cao, W. Chen, J. Zhang, W. Liu, G. Yang, X. Di, T. Ryder, Z. He, U. Surti, M.S. Phillips, M.T. Boyce-Jacino, S.P. Fodor, K.W. Jones, Large-scale genotyping of complex DNA, Nat. Biotechnol. 21 (2003) 1233–1237.
[5] Y. Nannya, M. Sanada, K. Nakazaki, N. Hosoya, L. Wang, A. Hangaishi, M. Kurokawa, S. Chiba, D.K. Bailey, G.C. Kennedy, S. Ogawa, A robust algorithm for copy number detection using high-density oligonucleotide single nucleotide polymorphism genotyping arrays, Cancer Res. 65 (2005) 6071–6079.
[6] Y. Inagaki, K. Yasui, M. Endo, T. Nakajima, K. Zen, K. Tsuji, M. Minami, S. Tanaka, M. Taniwaki, Y. Itoh, S. Arii, T. Okanoue, CREB3L4, INTS3, and SNAPAP are targets for the 1q21 amplicon frequently detected in hepatocellular carcinoma, Cancer Genet. Cytogenet. 180 (2008) 30–36.
[7] K. Yasui, I. Imoto, Y. Fukuda, A. Pimkhaokham, Z.Q. Yang, T. Naruto, Y. Shimada, Y. Nakamura, J. Inazawa, Identification of target genes within an amplicon at 14q12–q13 in esophageal squamous cell carcinoma, Genes Chromosomes Cancer 32 (2001) 112–118.
[8] C. Collins, J.M. Rommens, D. Kowbel, T. Godfrey, M. Tanner, S.I. Hwang, D. Polikoff, G. Nonet, J. Cochran, K. Myambo, K.E. Jay, J. Froula, T. Cloutier, W.L. Kuo, P. Yaswen, S. Dairkee, J. Giovanola, G.B. Hutchinson, J. Isola, O.P. Kallioniemi, M. Palazzolo, C. Martin, C. Ericsson, D. Pinkel, D. Albertson, W.B. Li, J.W. Gray, Positional cloning of ZNF217 and NABC1: genes amplified at 20q13.2 and overexpressed in breast carcinoma, Proc. Natl. Acad. Sci. USA 95 (1998) 8703–8708.
[9] E.A. Cox, S.K. Sastry, A. Huttenlocher, Integrin-mediated adhesion regulates cell polarity and membrane protrusion through the Rho family of GTPases, Mol. Biol. Cell 12 (2001) 265–277.
[10] C. Sakakura, A. Hagiwara, H. Taniguchi, T. Yamaguchi, H. Yamagishi, T. Takahashi, K. Koyama, Y. Nakamura, T. Abe, J. Inazawa, Chromosomal aberrations in human hepatocellular carcinomas associated with hepatitis C virus infection detected by comparative genomic hybridization, Br. J. Cancer 80 (1999) 2034–2039.
[11] Y.J. Chen, J.Y. Ko, P.J. Chen, C.H. Shu, M.T. Hsu, S.F. Tsai, C.H. Lin, Chromosomal aberrations in nasopharyngeal carcinoma analyzed by comparative genomic hybridization, Genes Chromosomes Cancer 25 (1999) 169–175.
[12] T. Yakut, H.J. Schulten, A. Demir, D. Frank, B. Danner, U. Egeli, C. Gebitekin, E. Kahler, B. Gunawan, N. Urer, H. Oztürk, L. Füzesi, Assessment of molecular events in squamous and non-squamous cell lung carcinoma, Lung Cancer 54 (2006) 293–301.
[13] P. Moinzadeh, K. Breuhahn, H. Stützer, P. Schirmacher, Chromosome alterations in human hepatocellular carcinomas correlate with aetiology and histological grade – results of an explorative CGH meta-analysis, Br. J. Cancer 92 (2005) 935–941.
[14] C. Schlaeger, T. Longerich, C. Schiller, P. Bewerunge, A. Mehrabi, G. Toedt, J. Kleeff, V. Ehemann, R. Eils, P. Lichter, P. Schirmacher, B. Radlwimmer, Etiology-dependent molecular mechanisms in human hepatocarcinogenesis, Hepatology 47 (2008) 511–520.
[15] S. Zrihan-Licht, Y. Fu, J. Settleman, K. Schinkmann, L. Shaw, I. Keydar, S. Avraham, H. Avraham, RAFTK/Pyk2 tyrosine kinase mediates the association of p190 RhoGAP with RasGAP and is involved in breast cancer cell invasion, Oncogene 19 (2000) 1318–1328.
[16] G. Chakravarty, D. Roy, M. Gonzales, J. Gay, A. Contreras, J.M. Rosen, P190-B, a Rho-GTPase-activating protein, is differentially expressed in terminal end buds and breast cancer, Cell Growth Differ. 11 (2000) 343–354.
[17] H. Nakahara, S.C. Mueller, M. Nomizu, Y. Yamada, Y. Yeh, W.T. Chen, Activation of beta1 integrin signaling stimulates tyrosine phosphorylation of p190RhoGAP and membrane-protrusive activities at invadopodia, J. Biol. Chem. 273 (1998) 9–12.
[18] X.D. Ren, W.B. Kiosses, M.A. Schwartz, Regulation of the small GTP-binding protein Rho by cell adhesion and the cytoskeleton, EMBO J. 18 (1999) 578–585.
[19] W.T. Arthur, K. Burridge, RhoA inactivation by p190RhoGAP regulates cell spreading and migration by promoting membrane protrusion and polarity, Mol. Biol. Cell 12 (2001) 2711–2720.
[20] K. Takaishi, T. Sasaki, M. Kato, W. Yamochi, S. Kuroda, T. Nakamura, M. Takeichi, Y. Takai, Involvement of Rho p21 small GTP-binding protein and its regulator in the HGF-induced cell motility, Oncogene 9 (1994) 273–279.
[21] A.J. Ridley, P.M. Comoglio, A. Hall, Regulation of scatter factor/hepatocyte growth factor responses by Ras, Rac, and Rho in MDCK cells, Mol. Cell. Biol. 15 (1995) 1110–1122.
[22] C.D. Nobes, A. Hall, Rho GTPases control polarity, protrusion, and adhesion during cell movement, J. Cell Biol. 144 (1999) 1235–1244.

Infrequent Amplification of *JUN* in Hepatocellular Carcinoma

MIO ENDO[1], KOHICHIROH YASUI[1], TOMOAKI NAKAJIMA[1], YASUYUKI GEN[1], KAZUHIRO TSUJI[1], OSAMU DOHI[1], KEIKA ZEN[1], HIRONORI MITSUYOSHI[1], MASAHITO MINAMI[1], YOSHITO ITOH[1], MASAFUMI TANIWAKI[2], SHINJI TANAKA[3], SHIGEKI ARII[3], TAKESHI OKANOUE[1,4] and TOSHIKAZU YOSHIKAWA[1]

Department of [1]Molecular Gastroenterology and Hepatology, and [2]Molecular Hematology and Oncology, Graduate School of Medical Science, Kyoto Prefectural University of Medicine, Kyoto; [3]Department of Hepato-Biliary-Pancreatic Surgery, Tokyo Medical and Dental University, Tokyo; [4]Center of Gastroenterology and Hepatology, Saiseikai Suita Hospital, Suita, Japan

Abstract. *Aim: To determine whether JUN (the oncogene encoding c-Jun protein) is amplified and overexpressed in hepatocellular carcinoma (HCC). Materials and Methods: DNA copy number aberrations were investigated using a high-density oligonucleotide microarray. DNA copy numbers were determined by fluorescence in situ hybridization. Genomic DNA and mRNA were quantified using real-time quantitative PCR. Results: A novel amplification was found at the chromosomal region 1p32-31 in a JHH-2 HCC cell line within which JUN is amplified and overexpressed. However, no copy number gain of JUN (>2-fold) was observed in 34 primary HCC tumors. Rather, a loss of JUN (<0.5-fold) was seen in 13 (38%) out of the 34 tumors and expression of JUN was significantly lower in 26 (70%) out of the 37 HCC tumors compared with their nontumorous counterparts. Conclusion: Although JUN was amplified and overexpressed in JHH-2 HCC cells, amplification and overexpression of JUN may be rare in primary HCCs.*

Hepatocellular carcinoma (HCC) is the fifth most common malignancy in men and the eighth most common in women worldwide and is estimated to cause approximately half a million deaths annually (1). Although the risk factors for HCC are well characterized, the molecular pathogenesis of this widespread type of cancer remains poorly understood (2). Amplification of DNA in specific chromosomal regions plays a crucial role in the development and progression of human malignancies, specifically when proto-oncogenic target genes within those amplicons are overexpressed. To identify genes potentially involved in HCC, we investigated DNA copy number aberrations in human HCC cell lines using high resolution single nucleotide polymorphism (SNP) arrays (3-5). We found that a novel amplification at the chromosomal region 1p32-31 occurs in HCC cell line and that the human oncogene *JUN*, which lies within the 1p32-31 amplicon, is amplified and overexpressed.

The oncogene *JUN* encodes the protein c-Jun, a component of the AP-1 transcriptional complex which regulates a wide range of cellular processes, including cell proliferation, death, survival and differentiation (6-8). *JUN* is the cellular homologue of *v-Jun*, the transforming oncogene of the avian sarcoma virus 17 (9, 10). Many experimental approaches have indicated that *JUN* plays an important role in carcinogenesis. Thus, *JUN* can transform mammalian cells, when coexpressed with an activated oncogene such as *Ras* or *Src* (11). Furthermore, transgenic mice expressing *JUN* develop osteosarcoma in cooperation with c-Fos (12). Recently, several lines of evidence have suggested that *JUN* is implicated in human cancer, including highly aggressive sarcomas (13), Hodgkin lymphomas (14) and acute myeloid leukemia (15). Amplification of *JUN* has also recently been described in highly aggressive sarcomas (13) and malignant pleural mesotheliomas (16). Most important in terms of this study, *JUN* also appears to be crucial for initiation of HCC development in a mouse model (17).

Therefore, overexpression of *JUN* following amplification may contribute to the initiation or progression of cancer, including HCC. In this study, based on the findings of the SNP-array analysis, we determined if *JUN* is indeed amplified and overexpressed in primary HCC tumors.

Materials and Methods

Cell lines and tumor samples. A total of 21 liver cancer cell lines (HCC-derived HLE, HLF, PLC/PRF/5, Li7, Huh7, Hep3B, SNU354, SNU368, SNU387, SNU398, SNU423, SNU449, SNU475, JHH-1, JHH-2, JHH-4, JHH-5, JHH-6, JHH-7, Huh1,

Correspondence to: Dr. Kohichiroh Yasui, Department of Molecular Gastroenterology and Hepatology, Graduate School of Medical Science, Kyoto Prefectural University of Medicine, 465 Kajii-cho, Kamigyo-ku, Kyoto 602-8566, Japan. Tel: +81 752515519, Fax: +81 752510710, e-mail: yasuik@koto.kpu-m.ac.jp

Key Words: Gene amplification, hepatocellular carcinoma, *JUN*.

0250-7005/2009 $2.00+.40

and the hepatoblastoma line HepG2) were obtained from the Health Science Research Resources Bank (Osaka, Japan) and the American Type Culture Collection (Manassas, VA, USA) and were examined as described previously (3). All cell lines were maintained in Dulbecco's modified Eagle's medium supplemented with 10% fetal calf serum. Paired tumor and nontumor tissues were obtained from 37 HCC patients who underwent surgery at the Hospital of Tokyo Medical and Dental University. All specimens were frozen immediately in liquid nitrogen and stored at −80°C until required. Genomic DNA was isolated using the Puregene DNA isolation kit (Gentra, Minneapolis, MN, USA) and total RNA was obtained using Trizol reagent (Invitrogen, Carlsbad, CA, USA). Thirty-four tumor samples were available for DNA analyses, and 37 paired tumor and nontumor samples were available for mRNA analyses. Prior to the study, informed consent was obtained and the study was approved by Ethics Committees.

SNP array. DNA copy number changes were analyzed by the GeneChip Mapping 100K array (Affymetrix, Santa Clara, CA, USA), as described previously (3). Copy number changes were calculated using the Copy Number Analyzer for Affymetrix GeneChip Mapping Arrays (CNAG; http://www.genome.umin.jp; (18).

Fluorescence in situ hybridization (FISH). FISH was performed using three bacterial artificial chromosomes (BACs), RP11-1040N24, RP11-63G10 and RP11-960H15 as probes (Invitrogen), as described previously (3). The BACs were selected based on their homology to locations in the human genome according to the database provided by the UCSC (http://genome.ucsc.edu/).

Real-time quantitative PCR. Genomic DNA and mRNA were quantified using a real-time fluorescence detection method, as described previously (3). The primers used were as follows: *JUN* DNA forward: 5'-CAGGTGGCACAGCTTAAACA-3', reverse: 5'-TTTTTCTCTCCGTCGCAACT-3'; *JUN* mRNA forward: 5'-CCCCAAGATCCTGAAACAGA-3', reverse: 5'-CCGTTGCTGGA CTGGATTAT-3'. These primers were designed using Primer3Plus (http://www.bioinformatics.nl/cgi-bin/primer3plus/ primer3plus.cgi) on the basis of sequence data obtained from the NCBI database (http://www.ncbi.nlm.nih.gov/). Endogenous controls for mRNA and genomic DNA levels were *GAPDH* and long interspersed nuclear element 1 (*LINE-1*), respectively.

Statistical analysis. All statistical analyses were performed using SPSS 15.0 software (SPSS Inc., Chicago, IL, USA). The Wilcoxon signed-rank test was used to compare *JUN* mRNA levels between tumorous and non-tumorous tissues. *P*-values of <0.05 were considered significant.

Results

Detection of 1p32-31 amplification in a JHH-2 HCC cell line by array analyses. Twenty HCC cell lines were screened for DNA copy number aberrations using Affymetrix GeneChip Mapping 100K array analysis. One of the 20 cell lines, JHH-2, exhibited a high-level copy-number gain that is indicative of gene amplification within the chromosomal region 1p32-31 (Figure 1A). The estimated extent of the region of amplification was 3.9 Mb. This chromosomal region lies between the Affymetrix markers SNP_A-1693528 and SNP_A-1722104 and contains 27 known or predicted protein-coding genes including *JUN* (Figure 1B). To confirm amplification of *JUN*, we performed FISH analyses on JHH-2 cells using the BACs RP11-1040N24, RP11-63G10 and RP11-960H15 as probes. The BAC RP11-63G10, which contains *JUN*, generated an amplified FISH signal (Figure 1D). In contrast, neither of the BACs RP11-1040N24 or RP11-960H15, which correspond to chromosomal regions outside of the amplicon, showed an amplified signal (Figure 1C and E).

DNA copy number and expression of JUN in liver cancer cell lines. Amplification of *JUN* was further determined by assay of the DNA copy number of *JUN* in 21 liver cancer cell lines (20 HCC cell lines and the hepatoblastoma line HepG2) by real-time quantitative PCR. For this analysis, the copy number values were normalized by assigning the copy number of genomic DNA derived from normal lymphocytes a value of 1. Copy number changes were counted as gains or losses if the copy number value for a given tumor cell was >2.0 or <0.5, respectively. A copy number gain-of-*JUN* was observed in 3 out of the 21 cell lines: JHH-2, JHH-7 and PLC/PRF/5 (Figure 2A). Loss of *JUN* was observed in 1 out of the 21 cell lines: Huh7 (Figure 2A).

A common criterion for the designation of a gene as a putative target of amplification is that its gene amplification leads to its overexpression (19). To determine whether gene amplification leads to overexpression of *JUN*, we assayed the mRNA level of *JUN* in the same 21 liver cancer cell lines by real-time quantitative PCR. *JUN* mRNA was overexpressed in 2 out of the 3 cell lines (JHH-2 and JHH-7 but not PLC/PRF/5) that had copy number gains of the *JUN* gene (Figure 2B). These findings suggested that *JUN* could be the target of the 1p32-31 amplicon.

DNA copy number and expression of JUN in primary HCC tumors. To determine if the amplification and overexpression of *JUN* that was observed in HCC cell lines was relevant to primary human carcinomas, we first determined the copy number of *JUN* in 34 primary HCCs using a similar method to that used for the HCC cell lines. No copy number gain of *JUN* (>2-fold) was observed in any of the tumors. Instead, a loss of *JUN* (<0.5-fold) was seen in 13 (38%) out of the 34 tumors (Figure 3A).

We next further assayed the mRNA level of *JUN* in paired tumor and nontumor tissues from 37 HCC patients (Figure 3B). The expression of *JUN* was significantly lower in 26 (70%) of the tumors compared with their nontumorous counterparts (Wilcoxon signed-rank test; p=0.002).

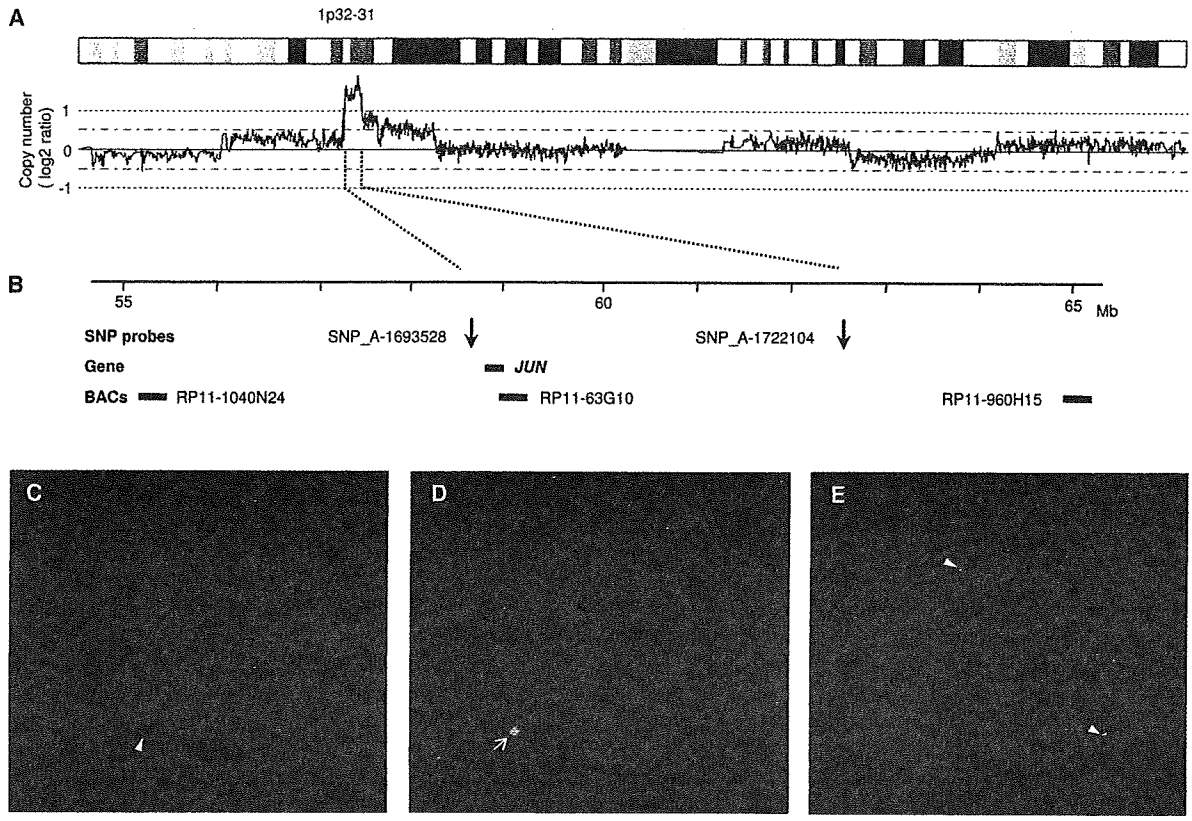

Figure 1. *Map of the amplicon at 1p32-31 in the JHH-2 cell line. A, Copy number profiles for chromosome 1 in JHH-2 cells. Copy number values were determined by SNP array analyses. B, The position of the Affymetrix SNP probes, the JUN gene and the three BACs chosen as probes for the FISH experiment based on the UCSC genome database (http://genome.ucsc.edu/) is shown. C-E, Representative images of FISH on metaphase chromosomes from JHH-2 cells using the following BAC probes: RP11-1040N24 (C), RP11-63G10 (D) and RP11-960H15 (E). RP11-63G10 shows an amplified signal (arrow; D), while RP11-1040N24 and RP11-960H15 show one copy and two copies per cell, respectively (arrowheads; C and E).*

Discussion

In the present study, we show that *JUN* is amplified and overexpressed in the JHH-2 HCC cell line. This cell line is derived from a Japanese HCC patient who was seronegative for hepatitis B virus (HBV) surface antigen (20). Furthermore, a copy number gain of *JUN* (>2-fold) was observed in 3 out of the 21 liver cancer cell lines (including JHH-2) that were tested and 2 of these 3 cell lines (JHH-2 and JHH-7) also showed enhanced mRNA expression of *JUN*. However, no copy number gain of *JUN* was observed in 34 primary HCC tumors that were examined. In fact, loss of *JUN* (<0.5-fold) was seen in 13 (38%) out of the 34 tumors. This loss of *JUN* in primary HCCs is consistent with previous studies that identified a frequent loss of DNA in HCCs at the chromosomal location where *JUN* resides (1p32-31) in comparative genomic hybridization and DNA microarray studies (21, 22). These findings suggest that amplification of *JUN* is rare in primary HCCs. However, the number of primary tumor samples examined in this study was relatively small. Further analysis of a greater number of primary samples is required to confirm the status of *JUN* amplification in primary HCCs.

The overall levels of the *JUN* protein product c-Jun are regulated by transcriptional and translational mechanisms and fine-tuning is achieved by post-translational modification, primarily by phosphorylation (23). Our analysis focused on *JUN* mRNA levels and further study is required to determine the mechanism and functional significance of the regulation of c-Jun protein levels in HCC. Real-time quantitative PCR analyses of primary HCC samples showed that expression of *JUN* mRNA is lower in tumors than in their nontumorous counterparts. These data are consistent with the fact that *JUN* is usually not overexpressed in human tumors (7). However, the low level of *JUN* in tumors does not necessarily imply that *JUN* does not have oncogenic potential in HCC. Several lines of evidence demonstrate a liver-specific function of *JUN* for cell survival and cell-cycle progression. *JUN* is essential for normal hepatogenesis during embryonic development (24, 25). Differentiated hepatocytes also require *JUN* for cell-cycle

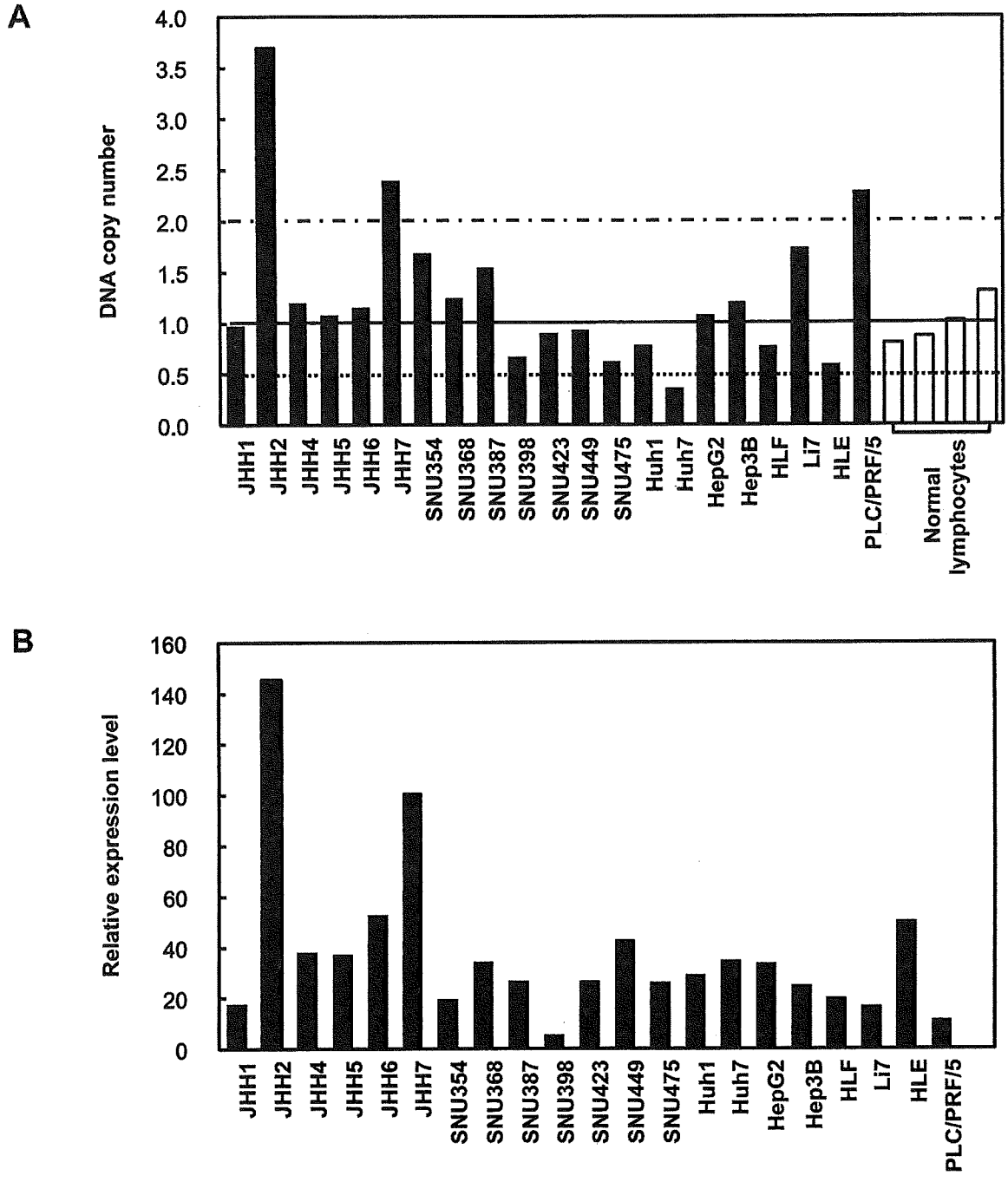

Figure 2. *DNA copy number and expression of JUN in liver cancer cell lines. A, DNA copy number of JUN in 21 liver cancer cell lines (20 HCC cells and one hepatoblastoma line HepG2) and four different peripheral blood lymphocyte samples (normal cell controls) was evaluated by real-time quantitative PCR with reference to LINE-1 controls. Values are normalized such that the average copy number in genomic DNA derived from normal lymphocytes has a value of 1 (solid horizontal line). A value greater than the cut-off value of 2, which represents a twofold increase in copy number over that of normal lymphocytes, was used to determine copy number gain and is shown as a broken line. A value less than the cut-off value of 0.5, which represents one half of the copy number of normal lymphocytes, was used to determine copy number loss and is shown as a dotted line. B, Relative expression levels of JUN in 21 liver cancer cell lines, as evaluated by real-time quantitative PCR, are shown. The results are presented as a ratio between the expression level of JUN and a reference gene (GAPDH) to correct for variation in the amount of RNA.*

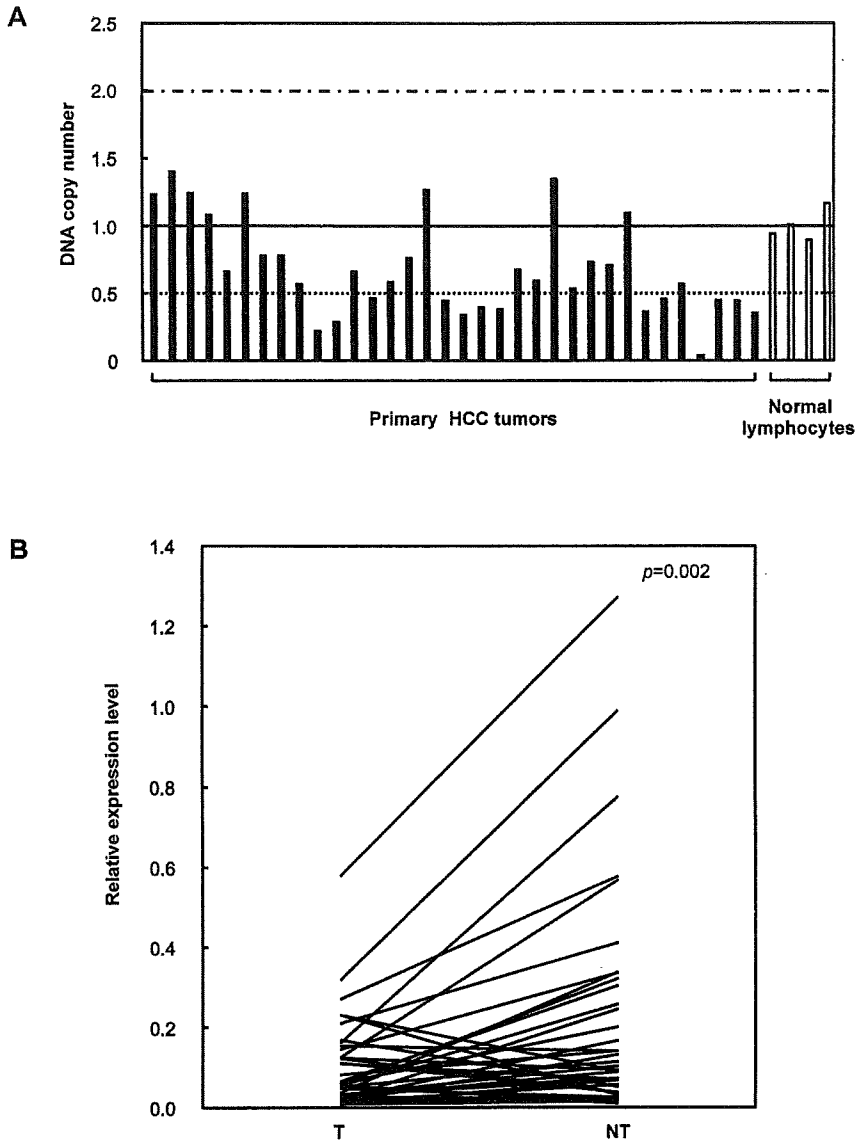

Figure 3. *DNA copy number and expression level of JUN in primary HCC tumors. A, The copy number of JUN in 34 primary HCC tumors and four normal peripheral blood lymphocyte samples was determined as described in the Materials and Methods Section. B, The relative expression of JUN in paired tumor (T) and nontumor tissues (NT) from 37 patients with primary HCC was determined as described in the Materials and Methods Section.*

progression since conditional knockout of *JUN* in adult livers reduced the proliferation capacity of hepatocytes after partial hepatectomy, a strong inducer of cell-cycle reentry (26).

However, the exact mechanism by which *JUN* contributes to tumorigenicity remains to be elucidated. *JUN* is located at the end of cellular signaling cascades that include oncogenes that are important for human tumorigenesis (7). The terminal position of *JUN* in cellular signaling pathways make *JUN* a participant in numerous and diverse mechanisms of oncogenesis. In order to fully understand the role of *JUN* in HCC it is therefore important to clarify the network of downstream target genes of *JUN* in HCC. Although our examination did not demonstrate the amplification of *JUN* in primary HCCs, the data presented in this work clearly show *JUN* amplification and overexpression in JHH-2 HCC cells. The JHH-2 cell line therefore provides an efficient tool for analyses of the relationship between *JUN* and oncogenesis.

Acknowledgements

This work was supported by Grants-in-Aid for Scientific Research (20590408) from the Japan Society for the Program of Science (to K.Y.).

References

1 Bosch FX, Ribes J, Cléries R and Díaz M: Epidemiology of hepatocellular carcinoma. Clin Liver Dis *9*: 191-211, 2005.

2 Thorgeirsson SS and Grisham JW: Molecular pathogenesis of human hepatocellular carcinoma. Nat Genet *31*: 339-346, 2002.

3 Inagaki Y, Yasui K, Endo M, Nakajima T, Zen K, Tsuji K, Minami M, Tanaka S, Taniwaki M, Itoh Y, Arii S and Okanoue T: *CREB3L4*, *INTS3*, and *SNAPAP* are targets for the 1q21 amplicon frequently detected in hepatocellular carcinoma. Cancer Genet Cytogenet *180*: 30-36, 2008.

4 Zen K, Yasui K, Nakajima T, Zen Y, Zen K, Gen Y, Mitsuyoshi H, Minami M, Mitsufuji S, Tanaka S, Itoh Y, Nakanuma Y, Taniwaki M, Arii S, Okanoue T and Yoshikawa T: ERK5 is a target for gene amplification at 17p11 and promotes cell growth in hepatocellular carcinoma by regulating mitotic entry. Genes Chromosomes Cancer *48*: 109-120, 2009.

5 Gen Y, Yasui K, Zen K, Nakajima T, Tsuji K, Endo M, Mitsuyoshi H, Minami M, Itoh Y, Tanaka S, Taniwaki M, Arii S, Okanoue T and Yoshikawa T: A novel amplification target, *ARHGAP5*, promotes cell spreading and migration by negatively regulating RhoA in Huh-7 hepatocellular carcinoma cells. Cancer Lett *275*: 27-34, 2009.

6 Shaulian E and Karin M: AP-1 as a regulator of cell life and death. Nat Cell Biol *4*: E131-136, 2002.

7 Vogt PK: Jun, the oncoprotein. Oncogene *20*: 2365-2377, 2001.

8 Jochum W, Passegué E and Wagner EF: AP-1 in mouse development and tumorigenesis. Oncogene *20*: 2401-2412, 2001.

9 Bohmann D, Bos TJ, Admon A, Nishimura T, Vogt PK and Tjian R: Human proto-oncogene c-*JUN* encodes a DNA-binding protein with structural and functional properties of transcription factor AP-1. Science *238*: 1386-1392, 1987.

10 Maki Y, Bos TJ, Davis C, Starbuck M and Vogt PK: Avian sarcoma virus 17 carries the *Jun* oncogene. Proc Natl Acad Sci USA *84*: 2848-2852, 1987.

11 Schütte J, Minna JD and Birrer MJ: Deregulated expression of human c-*Jun* transforms primary rat embryo cells in cooperation with an activated c-Ha-*ras* gene and transforms rat-1a cells as a single gene. Proc Natl Acad Sci USA *86*: 2257-2261, 1989.

12 Wang ZQ, Liang J, Schellander K, Wagner EF and Grigoriadis AE: c-*Fos*-induced osteosarcoma formation in transgenic mice: cooperativity with c-*Jun* and the role of endogenous c-*Fos*. Cancer Res *55*: 6244-6251, 1995.

13 Mariani O, Brennetot C, Coindre JM, Gruel N, Ganem C, Delattre O, Stern MH and Aurias A: *JUN* oncogene amplification and overexpression block adipocytic differentiation in highly aggressive sarcomas. Cancer Cell *11*: 361-374, 2007.

14 Mathas S, Hinz M, Anagnostopoulos I, Krappmann D, Lietz A, Jundt F, Bommert K, Mechta-Grigoriou F, Stein H, Dörken B and Scheidereit C: Aberrantly expressed c-Jun and JunB are a hallmark of Hodgkin lymphoma cells, stimulate proliferation and synergize with NF-κB. EMBO J *21*: 4104-4113, 2002.

15 Rangatia J, Vangala RK, Singh SM, Peer Zada AA, Elsässer A, Kohlmann A, Haferlach T, Tenen DG, Hiddemann W and Behre G: Elevated c-Jun expression in acute myeloid leukemias inhibits C/EBPα DNA binding *via* leucine zipper domain interaction. Oncogene *22*: 4760-4764, 2003.

16 Taniguchi T, Karnan S, Fukui T, Yokoyama T, Tagawa H, Yokoi K, Ueda Y, Mitsudomi T, Horio Y, Hida T, Yatabe Y, Seto M and Sekido Y: Genomic profiling of malignant pleural mesothelioma with array-based comparative genomic hybridization shows frequent non-random chromosomal alteration regions including *JUN* amplification on 1p32. Cancer Sci *98*: 438-446, 2007.

17 Eferl R, Ricci R, Kenner L, Zenz R, David JP, Rath M and Wagner EF: Liver tumor development. c-Jun antagonizes the proapoptotic activity of p53. Cell *112*: 181-192, 2003.

18 Nannya Y, Sanada M, Nakazaki K, Hosoya N, Wang L, Hangaishi A, Kurokawa M, Chiba S, Bailey DK, Kennedy GC and Ogawa S: A robust algorithm for copy number detection using high-density oligonucleotide single nucleotide polymorphism genotyping arrays. Cancer Res *65*: 6071-6079, 2005.

19 Collins C, Rommens JM, Kowbel D, Godfrey T, Tanner M, Hwang SI, Polikoff D, Nonet G, Cochran J, Myambo K, Jay KE, Froula J, Cloutier T, Kuo WL, Yaswen P, Dairkee S, Giovanola J, Hutchinson GB, Isola J, Kallioniemi OP, Palazzolo M, Martin C, Ericsson C, Pinkel D, Albertson D, Li WB and Gray JW: Positional cloning of *ZNF217* and *NABC1*: genes amplified at 20q13.2 and overexpressed in breast carcinoma. Proc Natl Acad Sci USA *95*: 8703-8708, 1998.

20 Fujise K, Nagamori S, Hasumura S, Homma S, Sujino H, Matsuura T, Shimizu K, Niiya M, Kameda H and Fujita K and Ohno T: Integration of hepatitis B virus DNA into cells of six established human hepatocellular carcinoma cell lines. Hepatogastroenterology *37*: 457-460, 1990.

21 Okamoto H, Yasui K, Zhao C, Arii S and Inazawa J: *PTK2* and *EIF3S3* genes may be amplification targets at 8q23-q24 and are associated with large hepatocellular carcinomas. Hepatology *38*: 1242-1249, 2003.

22 Katoh H, Ojima H, Kokubu A, Saito S, Kondo T, Kosuge T, Hosoda F, Imoto I, Inazawa J, Hirohashi S and Shibata T: Genetically distinct and clinically relevant classification of hepatocellular carcinoma: putative therapeutic targets. Gastroenterology *133*: 1475-1486, 2007.

23 Vogt PK and Bader AG: Jun: stealth, stability, and transformation. Mol Cell *19*: 432-433, 2005.

24 Hilberg F, Aguzzi A, Howells N and Wagner EF: c-Jun is essential for normal mouse development and hepatogenesis. Nature *365*: 179-181, 1993.

25 Eferl R, Sibilia M, Hilberg F, Fuchsbichler A, Kufferath I, Guertl B, Zenz R, Wagner EF and Zatloukal K: Functions of c-Jun in liver and heart development. J Cell Biol *145*: 1049-1061, 1999.

26 Behrens A, Sibilia M, David JP, Möhle-Steinlein U, Tronche F, Schütz G and Wagner EF: Impaired postnatal hepatocyte proliferation and liver regeneration in mice lacking c-*Jun* in the liver. EMBO J *21*: 1782-1790, 2002.

Received July 16, 2009
Revised November 3, 2009
Accepted November 5, 2009

Liver International ISSN 1478-3223

CLINICAL STUDIES

Oxidative stress may enhance the malignant potential of human hepatocellular carcinoma by telomerase activation

Taichiro Nishikawa, Tomoki Nakajima, Tatsuo Katagishi, Yoshihisa Okada, Masayasu Jo, Keizo Kagawa, Takeshi Okanoue, Yoshito Itoh and Toshikazu Yoshikawa

Kyoto Prefectural University of Medicine Graduate School of Medical Science, Molecular Gastroenterology and Hepatology, Kyoto, Japan

Keywords
Akt – 8-OHdG – HCC – hTERT – PTEN – telomere

Abbreviations
DAPI, 4-6-diamidino-2-phenylindole; 8-OhdG, 8-hydroxy-2′-deoxyguanosine; FITC, fluorescein isothiocyanate; HCC, human hepatocellular carcinoma; hTERT, human telomerase reverse transcriptase; OS, oxidative stress; PNA, peptide nucleic acid; PTEN, phosphatase and tensin homolog deleted on chromosome 10; ROS, reactive oxygen species; RTA, relative telomerase activity; TRAP, telomere repeat amplification protocol.

Correspondence
Taichiro Nishikawa, Kyoto Prefectural University of Medicine Graduate School of Medical Science, Molecular Gastroenterology and Hepatology, Kyoto, Japan
Tel: +81 75 251 5519
Fax: +81 75 251 0710
e-mail: liverresearch2004@yahoo.co.jp

Received 2 September 2008
Accepted 7 November 2008

DOI:10.1111/j.1478-3231.2008.01963.x

Abstract

Background/Aims: Continuous oxidative stress (OS) plays an important role in the progression of chronic liver diseases and hepatocarcinogenesis through telomere shortening in hepatocytes. However, it has not been established how the OS influences the progression of human hepatocellular carcinomas (HCCs). We examined the correlations of OS with telomere length of cancer cells, telomerase activity and other clinicopathological factors in 68 HCCs. *Methods:* The level of 8-hydroxy-2′-deoxyguanosine (8-OHdG) as a marker of OS was examined immunohistochemically and OS was scored in four grades (0–3). The telomere length of cancer cells was measured by quantitative fluorescence *in situ* hybridization. Telomerase activity was measured by (i) immunodetection of human telomerase reverse transcriptase (hTERT) and (ii) telomere repeat amplification protocol (TRAP) assay. Telomerase related proteins, phosphatase and tensin homolog deleted on chromosome 10 (PTEN) and Akt, and other clinicopathological factors were also evaluated. *Results:* As the OS grade increased, the average telomere length became significantly shorter in HCCs, especially in the hTERT-negative group. In the state of high-grade OS, hTERT-positive HCC cells showed more proliferative and less apoptotic features compared with hTERT-negative HCC cells. Telomerase activity, as measured by the TRAP assay, was strongly correlated with OS grade in HCCs. Furthermore, a high OS grade was correlated with the downexpression of PTEN and the activation of Akt. *Conclusions:* Oxidative stress enhanced the malignant potential of HCCs through the activation of telomerase, which raises the possibility of using OS as a marker for assessing the clinical state of HCCs.

Continuous oxidative stress (OS), which results from the generation of reactive oxygen species (ROS) by environmental factors or cellular mitochondrial dysfunction, has recently been associated with the progression of chronic liver diseases and hepatocarcinogenesis (1–3). Repeated necrosis and regeneration of hepatocytes induced by OS appear to accelerate the senescence of hepatocytes, giving them the appearance of cancer cells. These processes may be due to the shortening of the telomeres of hepatocytes.

Telomeres, hexameric DNA repeats $(TTAGGG)_n$ at the ends of chromosomes (4), increase chromosomal stability by preventing chromosomal rearrangements and end-to-end fusions. In normal somatic cells, telomere shortening occurs during each cell division (5) and eventually leads to cell cycle arrest and apoptosis (6). In cancer cells, the length of telomeres is maintained by the expression of telomerase, which endows cancer cells with immortality and an ability to proliferate without any limit.

OS accelerates the shortening of the telomeres of human cells by inducing oxidative single-stranded damage in telomeric DNA (7, 8). Fibrosis and cirrhosis in liver have been attributed to OS-induced telomere shortening (9, 10). In hepatocytes, telomere shortening can be carcinogenic because it can lead to genetic changes such as telomerase activation (11). Whereas OS has such effects on normal liver cells, it is unclear whether it also has a role in the progression of hepatic cancer cells, especially with respect to telomeres and telomerase.

In this study, we investigated the effects of OS in human hepatocellular carcinomas (HCCs). Our findings indicate that OS promotes the development of HCCs and increases

their resistance to treatment and is associated with shortened telomeres and increased telomerase activity.

Materials and methods

Tissue preparation and patients

All HCC specimens were obtained from 63 patients who underwent partial hepatectomy and five patients who underwent needle biopsy in 1992–2005 in Kyoto Prefectural University of Medicine. None of the specimens had undergone any treatments such as percutaneous ethanol injection therapy or transcatheter arterial embolization before the collections. The clinicopathological parameters of these patients and the clinicopathological status of their HCC samples are shown in Table 1. Fourteen patients were positive for serum hepatitis B surface antigen, 45 were positive for anti-hepatitis C antibody, one was positive for both and eight were negative for both. Of the 68 patients, two had normal livers, 29 had chronic hepatitis and 37 had liver cirrhosis. Specimens were fixed in 4% buffered paraformaldehyde for 12–24 h, embedded in paraffin and cut into 5-μm-thick sections for use as described below. All 68 HCC paraffin blocks included non-cancerous tissues, which served as controls. Additionally, parts of 30 specimens were stored at − 80 °C for later use in the telomere repeat amplification protocol (TRAP) assay (described below). Sixty-eight HCC specimens were stained with haematoxylin and eosin and classified according to their differentiation status according to the criteria of the Liver Cancer Study Group of Japan. Of these specimens, 29 were classified as well differentiated, 28 were classified as moderately differentiated and 11 were classified as poorly differentiated. The degree of necroinflammatory activity and fibrosis of non-cancerous tissues were classified according to the international classification (12) by haematoxylin and eosin and Masson trichrome staining. Informed consent to our using HCC specimens for this study was obtained from all patients according to the guidelines approved by our hospital ethical committee.

Table 1. Age and sex of 68 human hepatocellular carcinoma patients and the clinicopathological status of their human hepatocellular carcinoma samples

Sex	
Male	43
Female	25
Age (years) (mean ± SD)	
Range	25–77
Mean ± SD	62.6 ± 8.15
Aetiology	
HBV	14
HCV	45
HBV+HCV	1
Non-HBV, non-HCV	8
Non-cancerous tissue	
Normal liver	2
Chronic hepatitis	29
Liver cirrhosis	37
Tumour size (mm)	12–160
Tumour stage	
I	10
II	46
III	9
IV	3
Tumour differentiation	
Well differentiated	29
Moderately differentiated	28
Poorly differentiated	11

HBV, hepatitis B virus; HCV, hepatitis C virus; SD, standard deviation.

Immunohistochemical analysis

Sections were deparaffinized, immersed in 0.3% H_2O_2–methanol for 20 min, autoclaved at 120 °C for 20 min in a Target Retrieval Solution (DakoCytomation, Kyoto, Japan), incubated in blocking buffer (Tris buffered saline containing 2% fetal bovine serum) to block non-specific reactions and incubated with one of the four primary antibodies diluted 1:100 in the blocking buffer at 4 °C overnight. The antibodies were mouse anti-Ki-67 monoclonal antibody (DakoCytomation), rabbit anti-phosphatase and tensin homolog deleted on chromosome 10 (PTEN) monoclonal antibody (Cell Signaling Technology Inc., Beverly, MA, USA) and rabbit anti-phospho-AKT (Ser473) monoclonal antibody (Cell Signaling Technology Inc.). The remaining procedure was based on the standard streptavidin–biotin–peroxidase complex method (13). Positive reactions were visualized using diaminobenzidine (DAB; Wako, Osaka, Japan) as a substrate. The sections were counterstained with haematoxylin. Each immunohistochemical analysis included a slide without the primary antibody as a negative control. The Ki-67 index, an indicator of tumoral proliferative activity, was defined as the number of Ki-67 antibody-positive cells per 1000 scored cancer cells.

8-Hydroxy-2′-deoxyguanosine immunohistochemistry

Following the method of Kato *et al.* (13), 1000–2000 cancer or normal hepatic cells from HCC or non-cancerous tissues were stained with antibody against 8-hydroxy-2′-deoxyguanosine (8-OhdG), a marker of oxidative DNA damage. Immunoreactive cells were detected as described above and were counted by two hepatologists (T. N. and T. N.). The degree of OS was classified according to the percentage of 8-OhdG-positive cells: Grade 0, < 10%; Grade 1, 10–50%; Grade 2, 50–90%; Grade 3, > 90%.

Human telomerase reverse transcriptase immunohistochemistry

Human telomerase reverse transcriptase (hTERT), a telomerase catalytic subunit, is an indicator of telomerase activity in cancer cells (14). hTERT was immunohistochemically detected with mouse anti-hTERT monoclonal antibody (Novocastra, Newcastle Upon Tyne, UK) as

described above. Lymphocytes, in which hTERT is normally strongly expressed (15), were used as a positive control.

Transferase-mediated deoxy uridine triphosphate nick end labelling

Apoptosis in HCC tissues was assessed using the transferase-mediated deoxy uridine triphosphate nick end-labelling technique (16). The signals were visualized with DAB and counterstained with haematoxylin. The apoptosis index was defined as the number of immunoreactive cells per 1000 scored cancer cells.

Telomere repeat amplification protocol assay

Telomerase activity was also semiquantitatively measured by a TRAP assay using a TRAPEZE Telomerase Detection Kit (Oncor, Gaithersburg, CA, USA) according to the manufacturer's protocol. Thirty frozen HCC samples were examined as described in supplementary method 1. Relative telomerase activities (RTAs) were classified into four groups: 0 (RTA was not detectable), 1+ ($0 < \text{RTA} < 50$), 2+ ($50 \leqq \text{RTA} < 100$) and 3+ ($100 \leqq \text{RTA}$).

Analysis of telomere length by quantitative fluorescence *in situ* hybridization

Telomeres were identified in the paraffin sections using a telomere-specific peptide nucleic acid fluorescence *in situ* hybridization kit as described previously (17). The sections were counterstained with 4′-6-diamidino-2-phenylindole (DAPI) (1000 ng/ml, VYS-32-804830, ABBOTT JAPAN CO., Tokyo, Japan). Following the protocol of Meeker *et al.* (18), image-processed telomeric signals were quantified from digitized fluorescence microscopic images using the image analysis software package IP LABS (version 3.54, Scanalytics, Fairfax, VA, USA). Lymphocytes were used as internal controls of the telomeric signal because the telomere lengths of the lymphocytes were less affected by ageing than those of somatic cells (19). The telomeric pixel intensities of 15–20 nuclei of cancer cells and 5–10 nuclei of lymphocytes were recorded. To correct the different amounts of DNA in the sectioned nuclei, the telomeric signal intensity was modified by dividing the pixel intensity of the telomere signal for a given nucleus by the pixel intensity of the DAPI signal within that nucleus, as reported previously (18). Average telomere length was defined as Tel-T/Tel-L, where Tel-T and Tel-L are the average modified telomeric signal intensities of cancer cells and lymphocytes, respectively, measured in four different fields per sample.

Statistical analysis

The data are represented as the mean and SD in each category. The correlations of OS grade in HCC tissues to different clinicopathological and biochemical factors were assessed using the Kruskal–Wallis H test, the Spearman's Rank Correlation Coefficient and the Mann–Whitney U test. Differences of clinicopathological factors between hTERT-negative and hTERT-positive HCCs were analysed using the Mann–Whitney U test. $P < 0.05$ was considered to be statistically significant. All the tests were analysed using the STATVIEW program (Abacus Concepts, Berkeley, CA, USA).

Results

Immunohistochemical analysis of 8-hydroxy-2′-deoxyguanosine in human hepatocellular carcinoma samples

HCC tissues representative of each OS grade are shown in Figure 1a. 8-OHdG was mainly found in the nuclei of cancer cells, but it was also found in the nuclei of lymphocytes and fibroblasts and hepatocytes in non-cancerous tissues. The OS grades of the HCC tissues were: 15 Grade 0, 17 Grade 1, 15 Grade 2 and 21 Grade 3. None of several clinicopathological parameters of the 68 subjects (age, sex, etc.) was significantly related to the OS grade (Table 2). Furthermore, no tumour factors (differentiation of HCC tissues, size, stage or etiology) was significantly related to the OS grade (Table 3). On the other hand, the OS grade of non-cancerous tissues was significantly related to the patient's age, etiology and grading of chronic hepatitis ($P < 0.05$, Kruskal–Wallis H test and Spearman's rank correlation coefficient, Table 4).

Immunohistochemical analysis of human telomerase reverse transcriptase in human hepatocellular carcinoma samples

hTERT, an indicator of telomerase activity in cancer cells (14), was immunodetected in lymphocytes, in which it is normally expressed (15) (Fig. 1b, left panel), and in some cancer cells, but not in other cells, including normal hepatocytes. hTERT in HCC cells was mainly localized in the nucleus, especially in the nucleolus (Fig. 1b, right panel). It was also weakly detected in the cytoplasm of HCCs (Fig. 1b, left panel). Of the 68 HCC specimens examined, 47 were judged hTERT-positive (strong detection) and 21 were judged hTERT-negative (no or weak detection) (Table 3).

Oxidative stress shortens telomere length in human hepatocellular carcinoma samples

The telomere signals of cancer cells and lymphocytes were detected as green fluorescein isothiocyanate signals within the blue DAPI signals (the nuclear signals of cancer cells and lymphocytes) (Fig. 1c). Extensive OS was found to significantly accelerate the shortening of telomeres in cancer cells ($P < 0.001$, Kruskal–Wallis H test, Table 3). As the OS grade increased, the average telomere length of cancer cells strongly decreased in hTERT-negative HCCs ($P < 0.001$) whereas it did not

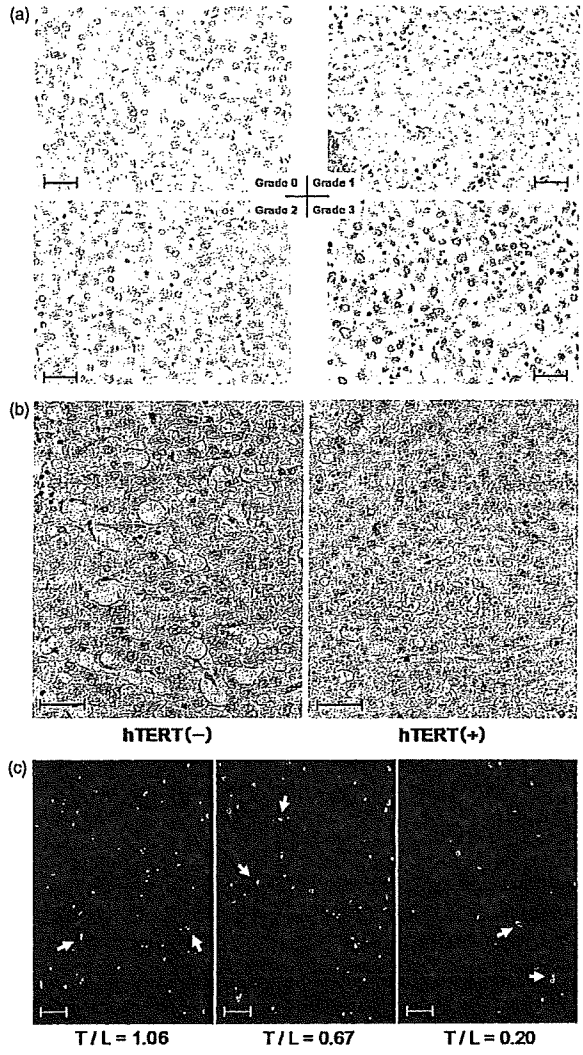

Fig. 1. Representative photographs of immunostaining and quantitative fluorescence *in situ* hybridization of human hepatocellular carcinoma (HCC) tissues. (a) Immunostaining of 8-hydroxy-2′-deoxyguanosine. The staining intensity was classified into four grades according to the percentage of immunoreactive cells. (b) Immunostaining of human telomerase reverse transcriptase (hTERT). In hTERT-negative HCCs, the cytoplasm of the cancer cell was faintly stained and the lymphocytes were strongly stained. In hTERT-positive HCCs, the nucleus, especially the nucleolus of the cancer cells, was strongly stained. (c) Representative photographs of quantitative fluorescence *in situ* hybridization for measurement of telomere length. White and red arrows in each photograph indicate the lymphocytes and the cancer cells in HCC tissues respectively. T/L below each photograph represents the average value of the mean Tel-T/mean Tel-L as the average telomere length of cancer cells in each HCC tissue, where mean Tel-T and mean Tel-L represent the average modified telomeric signal intensity of cancer cells and lymphocytes respectively. Scale bars, 50 μm.

significantly change in hTERT-positive HCCs (Fig. 2a). The difference between the average telomere lengths in hTERT-positive and hTERT-negative HCCs significantly increased with increasing OS grade ($P < 0.05$, Mann–Whitney U test, Fig. 2b).

Oxidative stress increases telomerase activity in human hepatocellular carcinoma samples

The immunodetection of hTERT in HCC tissues was significantly correlated with OS grade ($P < 0.001$, Kruskal–Wallis H test, Fig. 2b). Additionally, samples with higher OS grades had higher RTA scores in the TRAP assay ($P < 0.05$, Spearman's rank correlation coefficient, Fig. 2c). The degree of tumour differentiation was significantly related to hTERT expression in HCC tissues but was not related to the length of telomeres (Table 5).

Increased proliferative activity and apoptotic resistance in human hepatocellular carcinoma samples by oxidative stress through telomerase activation

We did not observe a correlation between the Ki-67 index, an indicator of tumoral proliferative activity, and OS grade in HCC tissues (Table 3), although we could not rule out the possibility that the Ki-67 index had a weak positive correlation with the OS grade in the hTERT-positive group and a weak negative correlation with the OS grade in the hTERT-negative group (Fig. 2d). On the other hand, OS was significantly correlated with the apoptosis index in HCC tissues ($P < 0.05$, Kruskal–Wallis H test, Table 3), especially in the hTERT-negative group ($P < 0.001$) (Fig. 2e). For OS Grades 2 and 3, the hTERT-positive HCC cells showed a significantly higher proliferative activity and a significantly higher apoptotic resistance than the hTERT-negative HCC cells ($P < 0.05$, Mann–Whitney U test, Fig. 2f). Additionally, malignancy parameters of HCC tissues (Ki-67 index, apoptosis index, differentiation and stage) were not significantly different between the OS Grades 0–1 and 2–3 groups in HCC tissues (Table 6). However, the Ki-67 index and differentiation were significantly different between the OS Grade 0–1 group and the OS Grade 2–3 and hTERT-positive group in HCC tissues ($P < 0.05$, Mann–Whitney U test, Table 6).

Downexpression of phosphatase and tensin homolog deleted on chromosome 10 and activated phosphorylation of AKT in human hepatocellular carcinoma samples by oxidative stress

Phospho-AKT (P-AKT), a regulator of telomerase activity (20, 21), was detected in the nucleus and the cytoplasm of cancer cells (Fig. 3a, panel A). PTEN, an inhibitor of Akt phosphorylation (22), was not detected in the same lesions (panel B). On the other hand, PTEN was detected strongly in the cytoplasm and weakly in the nucleus in cancer cells that were P-AKT negative (panels C and D). Staining of PTEN was stronger in the non-cancerous part of an HCC sample (N in panel E) than in the cancerous part (T), as reported previously (23). As

Table 2. The correlation between the oxidative stress grades of 68 human hepatocellular carcinoma samples and the clinicopathological parameters of their human hepatocellular carcinoma patients

	8-OHdG				
	Grade 0 ($n=15$)	Grade 1 ($n=17$)	Grade 2 ($n=15$)	Grade 3 ($n=21$)	*P*-value
Sex (M/F)	11/4	11/7	10/6	11/10	0.5808
Age (years)	61.9 ± 8.4	64.1 ± 6.3	59.3 ± 13.0	63.6 ± 6.3	0.6465
BMI (kg/m^2)	22.9 ± 3.6	23.7 ± 2.7	21.9 ± 3.2	24.0 ± 2.3	0.3415
AST (IU/L)	63.4 ± 35.1	62.9 ± 43.5	62.5 ± 42.9	45.5 ± 22.7	0.5273
ALT (IU/L)	70.3 ± 39.8	53.6 ± 29.0	58.3 ± 42.1	40.8 ± 23.0	0.1700
PLT (× 10^4/μl)	13.6 ± 6.3	12.8 ± 4.8	13.4 ± 6.3	12.9 ± 7.1	0.9507
ALB (g/dl)	3.85 ± 0.49	4.20 ± 0.47	4.15 ± 0.28	4.15 ± 0.43	0.2689
ICG15 (%)	22.8 ± 13.5	13.9 ± 8.1	17.5 ± 12.1	14.6 ± 12.1	0.2684
AFP (μg/ml)	5860 ± 19 708	7458 ± 2215	294 ± 897	11 936 ± 46 136	0.7615
PIVKA-II (mAU/ml)	1211 ± 4372	1936 ± 5316	334 ± 510	394 ± 1113	0.9807

Data are expressed as mean ± SD.

Statistical analysis was performed using the Kruskal–Wallis *H*-test.

ALB, albumin; ALT, alanine aminotransferase; AFP, á-foetoprotein ; AST, aspartate aminotransferase; BMI, body mass index; 8-OHdG, 8-hydroxy-2′-deoxyguanosine; F, female; ICG, indocyanine green; M, male; PLT, platelet; SD, standard deviation.

Table 3. Correlations between the oxidative stress grades of 68 human hepatocellular carcinoma samples and clinicopathological factors

	8-OHdG				
	Grade 0 ($n=15$)	Grade 1 ($n=17$)	Grade 2 ($n=15$)	Grade 3 ($n=21$)	*P*-value
T-length (T/L)	1.097 ± 0.198	0.599 ± 0.271	0.549 ± 0.209	0.822 ± 0.663	0.00008110**
hTERT (N/P)	15/0	15/2	10/5	7/14	0.00006758**
Telomerase (0/1/2/3)	2/3/0/0	1/4/1/0	2/2/3/1	0/4/5/2	0.002539*
Ki-67 index	13.41 ± 8.43	13.41 ± 7.14	14.74 ± 9.87	15.75 ± 9.09	0.8654
Apo index	1.218 ± 0.720	1.782 ± 0.913	2.526 ± 1.372	2.306 ± 1.976	0.04040*
Different (W/M/P)	9/5/1	7/8/2	7/5/3	6/10/5	0.05515
Size (mm)	44.53 ± 43.00	49.47 ± 37.81	45.86 ± 36.17	41.95 ± 20.12	0.5474
Stage (I/II/III/IV)	5/7/3/0	4/5/7/1	1/11/3/0	3/14/2/2	0.6141
Aetiology (B/C/B+C/NBNC)	3/9/1/2	2/13/0/2	5/9/0/1	4/14/0/3	0.5311
Non-tumour (N/CH/LC)	1/5/9	0/9/8	1/5/9	0/12/9	0.2674

Data are expressed as mean ± SD.

Statistical analysis was performed using the Spearman's rank correlation coefficient in telomerase, differentiation, stage and non-tumour and using the Kruskal–Wallis *H*-test in other factors.

*$P < 0.05$.

**$P < 0.001$.

Apo index, apoptosis index; B/C/B+C/NBNC, HBV/HCV/HBV+HCV/non-HBV, non-HCV; Different, tumour differentiation; 8-OHdG, 8-hydroxy-2′-deoxyguanosine; HBV, hepatitis B virus; HCV, hepatitis C virus; hTERT, human telomerase reverse transcriptase; N/P, negative/positive; NL/CH/LC, normal liver/chronic hepatitis/liver cirrhosis; SD, standard deviation; T-length, telomere length; T/L, tumour cell/lymphocyte; W/M/P, well differentiated/moderately differentiated/poorly differentiated.

the OS grade increased, the level of Akt phosphorylation in HCC samples increased significantly ($P < 0.001$, Fig. 3b) and the expression of PTEN in HCC samples decreased significantly ($P < 0.05$, Fig. 3b). These results suggest that the activation of telomerase by OS in HCC tissues is due to the downexpression of PTEN and the following activation of Akt.

Discussion

Although OS has been associated with chronic liver disease (24, 25), whether it has a role in the clinicopathology of HCC has not been investigated previously. In the present study, most HCC tissues (53/68, 77.9%) had high levels of OS (OS grades over 1). However, the 8-OHdG levels in the cancerous parts were not significantly related to those in the non-cancerous parts (Table 4). This suggests that the cause of OS in HCC cells is different from that in hepatocytes in chronic liver diseases.

Furthermore, the OS grade in HCC tissues was not significantly correlated with several clinicopathological factors of HCC samples, such as degree of differentiation, size, stage, etiology and type of non-cancerous tissue

Table 4. The correlation between the oxidative stress grades of 68 non-cancerous tissues and the clinicopathological parameters of their patients

	8-OHdG				
	Grade 0 ($n=14$)	Grade 1 ($n=22$)	Grade 2 ($n=19$)	Grade 3 ($n=13$)	*P*-value
Sex (M/F)	9/5	13/9	10/9	10/3	0.6944
Age (years)	60.0 ± 6.4	60.2 ± 9.4	66.1 ± 7.0	64.2 ± 7.2	0.04901*
BMI (kg/m^2)	23.5 ± 2.1	21.9 ± 2.8	23.9 ± 2.7	24.1 ± 2.7	0.1493
AST (IU/L)	61.0 ± 46.0	58.2 ± 36.3	57.1 ± 36.3	66.0 ± 33.6	0.7817
ALT (IU/L)	60.5 ± 38.5	53.0 ± 29.8	54.6 ± 40.1	65.4 ± 37.8	0.7232
PLT (× 10^4/μl)	13.9 ± 8.5	12.4 ± 5.8	14.8 ± 4.9	12.0 ± 5.4	0.2568
ALB (g/dl)	4.12 ± 0.28	4.11 ± 0.55	4.05 ± 0.45	4.18 ± 0.32	0.7337
ICG15 (%)	22.8 ± 13.5	13.9 ± 8.1	17.5 ± 12.1	14.6 ± 12.1	0.2684
Aetiology (B/C/B+C/NBNC)	5/9/0/0	8/12/2/0	1/14/3/1	0/11/2/0	0.01378*
Grading (A0/A1/A2/A3)	0/11/2/1	0/12/9/1	1/8/9/1	1/2/5/5	0.003754*
Staging (F0/F1/F2/F3/F4)	0/2/4/0/8	0/2/4/6/10	1/1/5/3/9	1/0/0/3/9	0.1893
OS tumour (G0/G1/G2/G3)	4/2/3/5	6/8/2/6	4/5/4/6	1/2/6/4	0.1679

Data are expressed as mean ± SD.

Statistical analysis was performed using the Spearman's rank correlation coefficient in grading, staging and OS tumour and using the Kruskal–Wallis *H*-test in other factors.

*$P < 0.05$.

ALB, albumin; ALT, alanine aminotransferase; AST, aspartate aminotransferase; B/C/B+C/NBNC, HBV/HCV/HBV+HCV/non-HBV, non-HCV; BMI, body mass index; 8-OHdG, 8-hydroxy-2′-deoxyguanosine; HBV, hepatitis B virus; HCC, human hepatocellular carcinoma; HCV, hepatitis C virus; ICG, indocyanine green; OS, oxidative stress; OS tumour, 8-OHdG grade of HCC tissue; PLT, platelet; SD, standard deviation.

(Table 3), although the OS grade in non-cancerous tissues was significantly correlated with several clinicopathological factors (Table 4). Tumour cells produce ROS at a far greater rate than do non-tumour cells *in vitro* and *in vivo* (26, 27). The increased ROS in HCC tissues may be due to hypoxia (28), which arises from the high proliferative activity and high cellular density of cancer cells. OS is also a mediator of angiogenesis signalling (29), which suggests that one of the effects of OS is to counteract the effects of hypoxia.

Our findings that OS in HCC tissues significantly accelerated telomere shortening and increased the apoptosis of cancer cells (Table 3) are consistent with our previous reports that OS hastened the telomere shortening of hepatocytes in chronic hepatitis C and non-alcoholic fatty liver disease (30, 31). Thus, OS appears to promote the senescence of cancer cells in HCC tissues through telomere shortening, as it does in hepatocytes in chronic liver diseases. OS also inhibits the proliferation of normal hepatocytes through telomere shortening (30). However, OS was not associated with the proliferative activity of HCC cells in this study, including hTERT-negative HCCs (Fig. 2d). Cancer cells with a high proliferative activity appear to be in a hypermetabolic state and appear to generate much cellular ROS. Additionally, the cell cycle checkpoint usually breaks down during carcinogenesis. Therefore, HCCs with high levels of OS may proliferate despite the OS-induced telomere shortening.

As the OS grade increased, the immunodetection of hTERT and telomerase activity in HCC tissues increased (Table 3). Although hTERT mRNAs were detected in the hepatocytes and in the serum of patients with chronic liver disease (32, 33), we were unable to detect hTERT protein in non-cancerous parts including liver tissues from patients with chronic hepatitis or liver cirrhosis. These results suggest that hTERT is immunodetected much more strongly in HCC tissues than in non-cancerous tissues. In agreement with previous reports (34, 35), HCC cells in the hTERT-positive group tended to have a higher proliferative activity and higher apoptotic resistance than did those in the hTERT-negative group, particularly in a highly oxidative-stressed environment (Fig. 2f). Additionally, HCC tissues with a high OS grade (2–3) and a high immunodetection of hTERT were significantly more proliferative and dedifferentiated than those with a low OS grade (0–1) (Table 6). Thus, OS in HCC tissues may increase the malignant potential of cancer cells by upregulating hTERT.

Although there is evidence that OS contributes to telomerase activation in HCC (36), the mechanism is unknown. In this study, we regarded the immunodetection of hTERT in the nucleus of cancer cells as an indicator of activated telomerase because the nuclear localization of hTERT is required to promote the elongation of telomere sequences within the cellular nucleus. hTERT must be phosphorylated before it can be translocated from the cytoplasm to the nucleus (37). Protein kinase B/Akt is known to be involved in the phosphorylation and the expression of hTERT (20, 21). Our finding that Akt is activated in HCC tissues with high-grade OS (Fig. 3b) is consistent with a report that OS increased the phosphorylation of Akt in human hepatoma cells *in vitro* (38). Additionally, the expression

of PTEN, a tumour suppressor and an inhibitor of the phosphorylation of Akt (22), significantly decreased in HCC tissues with increasing OS grade (Fig. 3b). OS may induce the inactivation of PTEN and the following activation of AKT in cancer cells (39). The downregulation and functional inactivation of PTEN may be a major mechanism of Akt phosphorylation by OS. Therefore, we assume that the PTEN–Akt pathway is a key factor in the activation of telomerase by OS in HCC tissues.

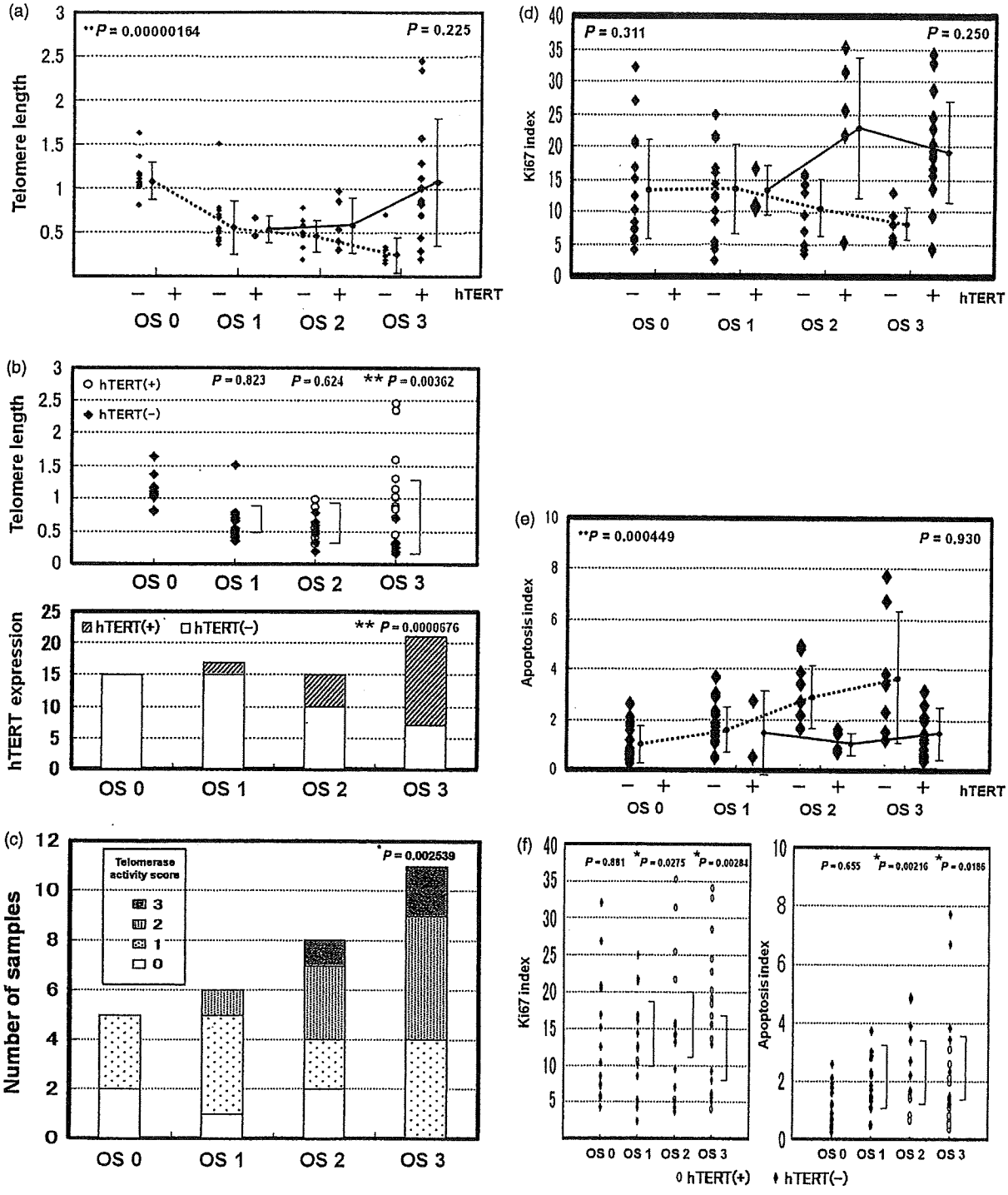

Liver International (2009)

Table 5. Human telomerase reverse transcriptase expression but not telomere length is related to the degree of tumour differentiation in 68 human hepatocellular carcinoma samples

	Histological grade of carcinoma			
Measurement	Well differentiated ($n = 15$)	Moderately differentiated ($n = 17$)	Poorly differentiated ($n = 15$)	*P*-value†
Telomere length‡	0.713 ± 0.329	0.835 ± 0.490	0.734 ± 0.653	0.4612
hTERT (N/P)§	24/5	18/10	5/6	0.01847*

†Statistical analysis was performed using the Kruskal–Wallis *H*-test.

‡Defined as T/L, where T and L are the telomere signal intensities of tumour cells and lymphocytes respectively. Data are expressed as mean ± SD.

§N/P, expression of hTERT in HCC tissues is negative/positive.

*$P < 0.05$.

HCC, human hepatocellular carcinoma; hTERT, human telomerase reverse transcriptase; SD, standard deviation.

Table 6. Correlations among the oxidative stress grade of human hepatocellular carcinomas, expression of human telomerase reverse transcriptase and clinicopathological factors

		Grades 2–3			
Measurement	Grades 0–1 ($n = 32$)	hTERT (−) ($n = 13$)	*P*-value	hTERT (+) ($n = 19$)	*P*-value
Ki-67 index	13.41 ± 7.65	15.33 ± 9.30	0.5349	20.57 ± 9.30	0.009035*
Apo index	3.591 ± 6.712	2.389 ± 1.695	0.2031	1.425 ± 0.886	0.3258
Differentiation (W/M/P)	16/13/1	13/15/8	0.05286	3/9/2	0.03283*
Stage (I/II/III/IV)	9/12/10/1	4/25/3/2	0.8865	0/14/3/2	0.3194

Data are expressed as mean ± SD.

Statistical analysis was performed using the Mann–Whitney *U*-test.

*$P < 0.05$.

Apo index, apoptosis index; differentiation, tumour differentiation; hTERT, human telomerase reverse transcriptase; W/M/P, well differentiated/moderately differentiated/poorly differentiated.

Our findings suggest that OS is associated with the malignant potential of HCCs through the activation of telomerase. Several drugs that are antioxidants are reported to prevent hepatocarcinogenesis and inhibit the growth of HCC cells (40, 41). We also recently demonstrated that epigallocatechin-3-gallate, a major polyphenol of green tea and a potent antioxidant, suppressed the growth of HCC cells *in vitro* and *in vivo* (42). These results raise the possibility of using antioxidant therapy to reduce OS in HCCs with high telomerase activity in order to inhibit the growth of HCCs. This is supported by the findings that the anticancer effects of antioxidants partially result from the downregulation of telomerase activity (43) and that inhibition of telomerase enhances the effects of chemotherapeutic agents in various cancer cells (44).

In conclusion, our findings show that HCC tissues are frequently characterized by OS, which contributes to the acceleration of telomere shortening and the activation of telomerase in cancer cells. The activation of telomerase by OS possibly results from the downexpression of PTEN and the phosphorylation of Akt. Because HCC cells that have high levels of hTERT as a result of OS are more malignant, continuous OS during the progression of HCCs may indicate a poor prognosis. Our results suggest that OS in HCC tissues can be used as a measure of the malignant potential.

Fig. 2. Oxidative stress (OS) accelerated telomere shortening, increased telomerase activity in human hepatocellular carcinoma (HCC) cells and was related to the increased proliferative activity and apoptotic resistance in HCC tissues through telomerase activation. (a) In human telomerase reverse transcriptase (hTERT)-negative HCCs, the average telomere length significantly decreased with increasing OS grade (dotted line) and in hTERT-positive HCCs, it elongated (solid line) (*$P < 0.05$, **$P < 0.001$ by the Kruskal–Wallis *H* test). (b) The average telomere length in hTERT-positive HCCs was elongated compared with those in hTERT-negative HCCs as the OS grade increased (upper) (by the Mann–Whitney *U* test). There was a positive correlation statistically between the OS grade and the expression of hTERT in HCC tissues (lower) (**$P < 0.001$ by the Kruskal–Wallis *H* test). (c) Distribution of telomerase activity among 30 HCC samples. Higher telomerase activity scores were more frequently observed in samples with higher OS grades (*$P < 0.05$ by Spearman's rank correlation coefficient). (d) The Ki-67 index in hTERT-negative HCCs (dotted line) and hTERT-positive HCCs (solid line) were not significantly affected by the OS grade (Kruskal–Wallis *H* test). (e) As the OS grade increased, the apoptosis index increased significantly in hTERT-negative HCCs (dotted line) but did not significantly change in hTERT-positive HCCs (solid line) (*$P < 0.05$, **$P < 0.001$ by the Kruskal–Wallis *H* test). (f) The Ki-67 index increased and the apoptosis index decreased in hTERT-positive HCCs compared with those in hTERT-negative HCCs, as the OS grade increased (*$P < 0.05$ by the Mann–Whitney *U* test). The data in (a), (d) and (e) show the mean and SD.

(a)

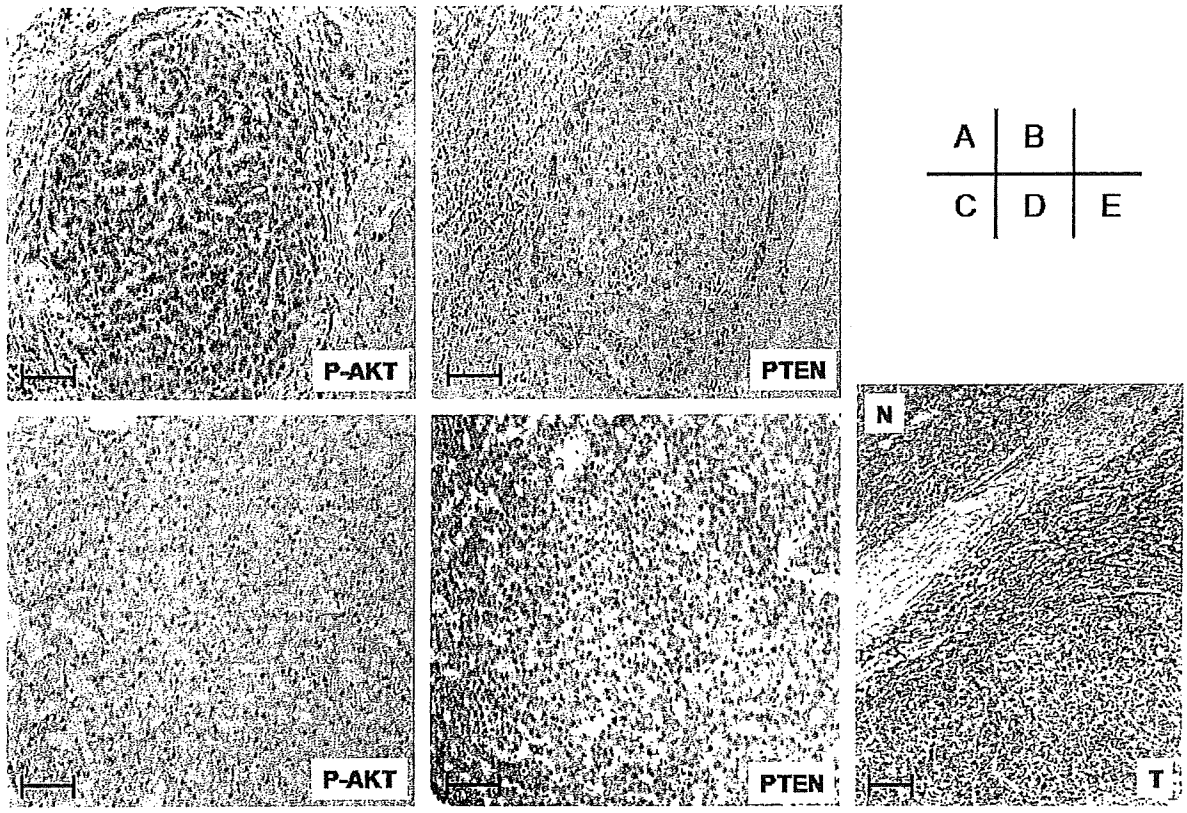

(b)

OS grade	P-AKT		PTEN	
	(–)	(+)	(–)	(+)
0 (*n*=15)	14	1	3	12
1 (*n*=17)	13	4	4	13
2 (*n*=15)	10	5	8	7
3 (*n*=21)	6	15	15	6
P-value	0.00013**		0.00435*	

Fig. 3. Oxidative stress (OS) increased the level of Akt phosphorylation and decreased the expression of phosphatase and tensin homolog deleted on chromosome 10 (PTEN) in human hepatocellular carcinoma (HCC) samples. (a) Representative photographs of immunostainings of phospho-Akt (P-AKT) in Ser473 and PTEN. P-AKT was detected in the nucleus and in the cytoplasm of cancer cells in the P-AKT-positive sample (A) and PTEN was not detected in the same lesion (B). Panel C shows a P-AKT-negative sample and PTEN was detected mainly in the cytoplasm of the cancer cells in the same lesion (D). Staining of PTEN was stronger in the non-cancerous part (N) than in the cancerous part (T) of the HCC sample (E). Scale bars, 50 μm. (b) The phosphorylation of Akt in HCC tissues significantly increased and the expression of PTEN in HCC tissues significantly decreased as the OS grade increased (*$P < 0.05$, **$P < 0.001$ by the Kruskal–Wallis *H* test).